

ENGINEERING OF BIOMATERIALS

INŻYNIERIA BIOMATERIAŁÓW

JOURNAL OF POLISH SOCIETY FOR BIOMATERIALS AND FACULTY OF MATERIALS SCIENCE AND CERAMICS AGH-UST

CZASOPISMO POLSKIEGO STOWARZYSZENIA BIOMATERIAŁÓW I WYDZIAŁU INŻYNIERII MATERIAŁOWEJ I CERAMIKI AGH

Number 156

Numer 156

Volume XXIII

Rok XXIII

JULY 2020

LIPIEC 2020

ISSN 1429-7248

PUBLISHER:

WYDAWCA:

**Polish Society
for Biomaterials
in Krakow**

Polskie
Stowarzyszenie
Biomateriałów
w Krakowie

**EDITORIAL
COMMITTEE:**

KOMITET

REDAKCYJNY:

Editor-in-Chief

Redaktor naczelny

Jan Chłopek

Editor

Redaktor

Elżbieta Pamuła

Secretary of editorial

Sekretarz redakcji

Design

Projekt

Katarzyna Trała

**ADDRESS OF
EDITORIAL OFFICE:**

ADRES REDAKCJI:

AGH-UST

30/A3, Mickiewicz Av.

30-059 Krakow, Poland

Akademia

Górniczno-Hutnicza

al. Mickiewicza 30/A-3

30-059 Kraków

Issue: 250 copies

Nakład: 250 egz.

**Scientific Publishing
House AKAPIT**

Wydawnictwo Naukowe

AKAPIT

e-mail: wn@akapit.krakow.pl



**EDITORIAL BOARD
KOMITET REDAKCYJNY**

EDITOR-IN-CHIEF

Jan Chłopek - AGH UNIVERSITY OF SCIENCE AND TECHNOLOGY, KRAKOW, POLAND

EDITOR

Elżbieta Pamuła - AGH UNIVERSITY OF SCIENCE AND TECHNOLOGY, KRAKOW, POLAND

**INTERNATIONAL EDITORIAL BOARD
MIĘDZYNARODOWY KOMITET REDAKCYJNY**

Iulian Antoniac - UNIVERSITY POLITEHNICA OF BUCHAREST, ROMANIA

Lucie Bacakova - ACADEMY OF SCIENCE OF THE CZECH REPUBLIC, PRAGUE, CZECH REPUBLIC

Romuald Będziński - UNIVERSITY OF ZIELONA GÓRA, POLAND

Marta Błażewicz - AGH UNIVERSITY OF SCIENCE AND TECHNOLOGY, KRAKOW, POLAND

Stanisław Błażewicz - AGH UNIVERSITY OF SCIENCE AND TECHNOLOGY, KRAKOW, POLAND

Maria Borczuch-Łączka - AGH UNIVERSITY OF SCIENCE AND TECHNOLOGY, KRAKOW, POLAND

Wojciech Chrzanowski - UNIVERSITY OF SYDNEY, AUSTRALIA

Jan Ryszard Dąbrowski - BIAŁYSTOK TECHNICAL UNIVERSITY, POLAND

Timothy Douglas - LANCASTER UNIVERSITY, UNITED KINGDOM

Christine Dupont-Gillain - UNIVERSITÉ CATHOLIQUE DE LOUVAIN, BELGIUM

Matthias Epple - UNIVERSITY OF DUISBURG-ESSEN, GERMANY

Robert Hurt - BROWN UNIVERSITY, PROVIDENCE, USA

James Kirkpatrick - JOHANNES GUTENBERG UNIVERSITY, MAINZ, GERMANY

Ireneusz Kotela - CENTRAL CLINICAL HOSPITAL OF THE MINISTRY OF THE INTERIOR AND ADMINISTR. IN WARSAW, POLAND

Małgorzata Lewandowska-Szumieł - MEDICAL UNIVERSITY OF WARSAW, POLAND

Jan Marciniak - SILESIA UNIVERSITY OF TECHNOLOGY, ZABRZE, POLAND

Ion N. Mihailescu - NATIONAL INSTITUTE FOR LASER, PLASMA AND RADIATION PHYSICS, BUCHAREST, ROMANIA

Sergey Mikhalovsky - UNIVERSITY OF BRIGHTON, UNITED KINGDOM

Stanisław Mitura - TECHNICAL UNIVERSITY OF LIBEREC, CZECH REPUBLIC

Piotr Niedzielski - TECHNICAL UNIVERSITY OF LODZ, POLAND

Abhay Pandit - NATIONAL UNIVERSITY OF IRELAND, GALWAY, IRELAND

Stanisław Pielka - WROCLAW MEDICAL UNIVERSITY, POLAND

Vehid Salih - UCL EASTMAN DENTAL INSTITUTE, LONDON, UNITED KINGDOM

Jacek Składzień - JAGIELLONIAN UNIVERSITY, COLLEGIUM MEDICUM, KRAKOW, POLAND

Andrei V. Stanishevsky - UNIVERSITY OF ALABAMA AT BIRMINGHAM, USA

Anna Ślósarczyk - AGH UNIVERSITY OF SCIENCE AND TECHNOLOGY, KRAKOW, POLAND

Tadeusz Trzaska - UNIVERSITY SCHOOL OF PHYSICAL EDUCATION, POZNAŃ, POLAND

Dimitris Tsipas - ARISTOTLE UNIVERSITY OF THESSALONIKI, GREECE

Wskazówki dla autorów

1. Prace do opublikowania w kwartalniku „Engineering of Biomaterials / Inżynieria Biomateriałów” przyjmowane będą wyłącznie w języku angielskim.

2. Wszystkie nadsyłane artykuły są recenzowane.

3. Materiały do druku prosimy przysyłać za pomocą systemu online (www.biomaterials.pl).

4. Struktura artykułu:

• TYTUŁ • Autorzy i instytucje • Streszczenie (200-250 słów) • Słowa kluczowe (4-6) • Wprowadzenie • Materiały i metody • Wyniki i dyskusja • Wnioski • Podziękowania • Piśmiennictwo

5. Autorzy przesyłają pełną wersję artykułu, łącznie z ilustracjami, tabelami, podpisami i literaturą w jednym pliku. Artykuł w tej formie przesyłany jest do recenzentów. Dodatkowo autorzy proszeni są o przesłanie materiałów ilustracyjnych (rysunki, schematy, fotografie, wykresy) w oddzielnych plikach (format np. .jpg, .gif, .tiff, .bmp). Rozdzielczość rysunków min. 300 dpi. Wszystkie rysunki i wykresy powinny być czarno-białe lub w odcieniach szarości i ponumerowane cyframi arabskimi. W tekście należy umieścić odnośniki do rysunków i tabel. W przypadku artykułów dwujęzycznych w tabelach i na wykresach należy umieścić opisy polskie i angielskie.

6. Na końcu artykułu należy podać wykaz piśmiennictwa w kolejności cytowania w tekście i kolejno ponumerowany.

7. Redakcja zastrzega sobie prawo wprowadzenia do opracowań autorskich zmian terminologicznych, poprawek redakcyjnych, stylistycznych, w celu dostosowania artykułu do norm przyjętych w naszym czasopiśmie. Zmiany i uzupełnienia merytoryczne będą dokonywane w uzgodnieniu z autorem.

8. Opinia lub uwagi recenzentów będą przekazywane Autorowi do ustosunkowania się. Nie dostarczenie poprawionego artykułu w terminie oznacza rezygnację Autora z publikacji pracy w naszym czasopiśmie.

9. Za publikację artykułów redakcja nie płaci honorarium autorskiego.

10. Adres redakcji:

Czasopismo

„Engineering of Biomaterials / Inżynieria Biomateriałów”

Akademia Górniczo-Hutnicza im. St. Staszica

Wydział Inżynierii Materiałowej i Ceramiki

al. Mickiewicza 30/A-3, 30-059 Kraków

tel. (48) 12 617 44 48, 12 617 25 61

tel./fax: (48) 12 617 45 41

e-mail: epamula@agh.edu.pl, kabe@agh.edu.pl

Szczegółowe informacje dotyczące przygotowania manuskryptu oraz procedury recenzowania dostępne są na stronie internetowej czasopisma:

www.biomaterials.pl

Warunki prenumeraty

Zamówienie na prenumeratę prosimy przysyłać na adres:

mgr inż. Augustyn Powroźnik

apowroz@agh.edu.pl, tel/fax: (48) 12 617 45 41

Cena pojedynczego numeru wynosi 20 PLN

Konto: Polskie Stowarzyszenie Biomateriałów

30-059 Kraków, al. Mickiewicza 30/A-3

ING Bank Śląski S.A. O/Kraków

nr rachunku 63 1050 1445 1000 0012 0085 6001

Prenumerata obejmuje 4 numery regularne i nie obejmuje numeru specjalnego (materiały konferencyjne).

Instructions for authors

1. Papers for publication in quarterly journal „Engineering of Biomaterials / Inżynieria Biomateriałów” should be written in English.

2. All articles are reviewed.

3. Manuscripts should be submitted to editorial office through online submission system (www.biomaterials.pl).

4. A manuscript should be organized in the following order:

• TITLE • Authors and affiliations • Abstract (200-250 words) • Keywords (4-6) • Introduction • Materials and Methods • Results and Discussions • Conclusions • Acknowledgements • References

5. All illustrations, figures, tables, graphs etc. preferably in black and white or grey scale should be additionally sent as separate electronic files (format .jpg, .gif, .tiff, .bmp). High-resolution figures are required for publication, at least 300 dpi. All figures must be numbered in the order in which they appear in the paper and captioned below. They should be referenced in the text. The captions of all figures should be submitted on a separate sheet.

6. References should be listed at the end of the article. Number the references consecutively in the order in which they are first mentioned in the text.

7. The Editors reserve the right to improve manuscripts on grammar and style and to modify the manuscripts to fit in with the style of the journal. If extensive alterations are required, the manuscript will be returned to the authors for revision.

8. Opinion or notes of reviewers will be transferred to the author. If the corrected article will not be supplied on time, it means that the author has resigned from publication of work in our journal.

9. Editorial does not pay author honorarium for publication of article.

10. Address of editorial office:

Journal

„Engineering of Biomaterials / Inżynieria Biomateriałów”

AGH University of Science and Technology

Faculty of Materials Science and Ceramics

30/A-3, Mickiewicz Av., 30-059 Krakow, Poland

tel. (48) 12) 617 44 48, 12 617 25 61

tel./fax: (48) 12 617 45 41

e-mail: epamula@agh.edu.pl, kabe@agh.edu.pl

Detailed information concerning manuscript preparation and review process are available at the journal's website:

www.biomaterials.pl

Subscription terms

Contact:

MSc Augustyn Powroźnik,

e-mail: apowroz@agh.edu.pl

Subscription rates:

Cost of one number: 20 PLN

Payment should be made to:

Polish Society for Biomaterials

30/A3, Mickiewicz Av.

30-059 Krakow, Poland

ING Bank Śląski S.A.

account no. 63 1050 1445 1000 0012 0085 6001

Subscription includes 4 issues and does not include special issue (conference materials).



29th Biomaterials in Medicine and Veterinary Medicine Annual Conference

15 – 18 October 2020 Rytro, Poland

SAVE THE DATE

15-18

OCTOBER
2020

www.biomat.agh.edu.pl



REGISTER
AND
SUBMIT
AN ABSTRACT



SPIS TREŚCI CONTENTS

- OPTIMIZING MANUFACTURING
CONDITIONS OF POLYMER
MICROSPHERES AS CELL CARRIERS
FOR MODULAR TISSUE ENGINEERING**
BARTOSZ MIELAN, ELŻBIETA PAMUŁA **2**
- EVALUATION OF THE STRENGTH
PROPERTIES OF MATERIALS INTENDED
FOR TRACHEOBRONCHIAL TUBES**
ROBERT SOBOTA, JAROSŁAW MARKOWSKI,
KAMIL JOSZKO, BOŻENA GZIK-ZROSKA,
EDYTA KAWLEWSKA, MAREK GZIK **10**
- COLLAGEN - STRUCTURE,
PROPERTIES AND APPLICATION**
ALEKSANDRA OW CZARZY, ROBERT KURASIŃSKI,
KAROLINA KULIG, WOJCIECH ROGÓŻ,
AGNIESZKA SZKUDLAREK,
MAŁGORZATA MACIĄŻEK-JURCZYK **17**
- THE INFLUENCE OF PROSTHETIC
ELEMENTS MANUFACTURING
TECHNOLOGY ON PROPERTIES
AND MICROSTRUCTURE SHAPING
Co-Cr-Mo ALLOYS**
JOANNA AUGUSTYN-NADZIEJA,
AGNIESZKA SZCZOTOK **24**

.....

WERSJA PAPIEROWA CZASOPISMA „ENGINEERING OF BIOMATERIALS / INŻYNIERIA BIOMATERIAŁÓW” JEST JEGO WERSJĄ PIERWOTNĄ
PRINTED VERSION OF „ENGINEERING OF BIOMATERIALS / INŻYNIERIA BIOMATERIAŁÓW” IS A PRIMARY VERSION OF THE JOURNAL

.....

OPTIMIZING MANUFACTURING CONDITIONS OF POLYMER MICROSPHERES AS CELL CARRIERS FOR MODULAR TISSUE ENGINEERING

BARTOSZ MIELAN , ELŻBIETA PAMUŁA* 

AGH UNIVERSITY OF SCIENCE AND TECHNOLOGY,
FACULTY OF MATERIALS SCIENCE AND CERAMICS,
DEPARTMENT OF BIOMATERIALS AND COMPOSITES,
AL. A. MICKIEWICZA 30, 30-059 KRAKÓW, POLAND
*E-MAIL: EPAMULA@AGH.EDU.PL

Abstract

Microspheres (MS) made of biostable polymer, namely polystyrene, have been used as substrates for cell culture enabling rapid cell expansion in dynamic conditions. However, due to non-resorbability, polystyrene (PS) MS when repopulated with cells cannot be directly used in tissue engineering. Our concept was to produce MS from resorbable polymer – poly(L-lactide-co-glycolide) (PLGA) as a support for adherent cells, e.g. osteoblasts. We hypothesize that such MS can be applied to the injured site to act as cell carriers or as modules for modular tissue engineering (MTE). In this article, we present the results of optimizing the PLGA MS manufacturing conditions via oil-in-water emulsification. Due to such a technique, MS with the required size, size distribution and properties suitable for cell culturing can be obtained. Three parameters of the oil-in-water emulsification were examined: the stirring speed of a water phase during MS manufacturing, the surfactant concentration, i.e. poly(vinyl alcohol) (PVA) in a water phase and concentration of PLGA in dichloromethane (DCM) as an oil phase. The results proved that the 7.5% PLGA concentration in DCM solution as an oil phase, the 0.5–2% concentration of PVA solution as a water phase and the stirring speed of water phase of 1000 rpm provided MS with the 160 μm mean diameter, which is suitable for cell culture. Moreover, the developed sieving and cleaning procedures were efficient to collect MS with the mean diameter of 280 μm, the more coherent size distribution and the ability to sink in the cell culture medium. The presence on the bottom of cell culture wells is crucial for MTE.

Keywords: modular tissue engineering, microspheres, cell culture, oil-in-water emulsification, poly(L-lactide-co-glycolide) (PLGA)

[*Engineering of Biomaterials* 156 (2020) 2-9]

doi:10.34821/eng.biomat.156.2020.2-9

Introduction

Apart from classical tissue engineering (TE) which uses macroscopic porous scaffolds seeded with cells, a new approach called modular tissue engineering (MTE) has recently been proposed [1]. The main idea of MTE is to mimic natural tissues and use microscale parts (named also microtissues) that can be assembled into bigger and more complex, dense and organomimetic structures [2–5].

These structures may form cell aggregates, cell sheets, or cells seeded on microcarriers and microspheres (MS). MS can be made of natural and synthetic materials (glass, polymer, ceramics) [6]. The most common MS that are used for the cell expansion in dynamic conditions are made of polystyrene (PS) [7]. With regard to MTE, the main advantage of PS MS is the high surface area accessible for cells in a comparatively low volume [8] while the disadvantage is non-resorbability.

Poly(L-lactide-co-glycolide) (PLGA) is widely used as a raw material for medical devices production as it has appropriate mechanical properties and is biocompatible with tissues in different applications. PLGA degrades by hydrolysis of ester bonds into oligomers and, finally, to monomer acids: lactic and glycolic which enter the Krebs cycle and are removed from the body as CO₂ and H₂O [9–10].

PLGA MS can be produced by various methods, such as: emulsification, spray-drying, phase separation, hot-melt extrusion, inkjet printing, gelation, grinding, coacervation, electrospay, supercritical fluid mixing, microfabrication [6].

The oil-in-water emulsification can be used to obtain PLGA MS on a laboratory scale and with multiple parameters controlled. It was reported that the increase in polymer molecular weight and its concentration in the oil phase raised the average MS diameter [11]. Increasing the oil phase volume in the water phase may slightly enlarge the MS diameter but their shape is less regular [12]. Also selecting a proper solvent is highly important the lower the boiling point of the organic solvent, the faster the MS formation [6]. The water phase also gives possibilities to control the emulsification process. For successful MS formation a surfactant addition is required. Poly(vinyl alcohol) (PVA) is commonly used and its concentration in the water phase may also affect the MS diameter – the higher PVA concentration in the water phase, the lower diameter and the narrower diameter distribution [6]. Additionally, the water phase volume increase can lower the MS diameter, however for very high values it causes the MS deformation [12].

The aim of our experiments was to optimize the PLGA MS manufacturing process so as to obtain two batches of particles with the diameters of ca. 150 μm and ca. 250 μm, respectively. In order to obtain MS with the desired mean diameter and the diameter distribution, three parameters were examined: the stirring speed of the water phase, the surfactant concentration, i.e. PVA in the water phase, and the PLGA concentration in the oil phase. The other parameters, such as: the oil and water phases volumes, the beaker and propeller geometry, the PLGA and PVA molecular weight, the lactide to glycolide ratio in PLGA, and the solvent type were constant and are not reported in this article, having been optimized during the preliminary studies. Dichloromethane (DCM) was chosen as a solvent due to its high volatility facilitating the faster MS formation. Additionally, the cleaning process was developed to dispose of the MS with the microstructure and properties inapplicable to cell cultures, e.g. MS with the high diameter dispersion or floating on the aqueous medium surface.

Materials and Methods

Materials

PLGA (85:15, M_n = 100 kDa, M_w = 210 kDa) was synthesized at the Center of Polymer and Carbon Materials, Polish Academy of Sciences, Zabrze, Poland and kindly provided by Prof. P. Dobrzyński. DCM (Avantor Performance Materials) and PVA (Mowiol® 4-88, M_w ca. 31 kDa, Sigma Aldrich) were used.

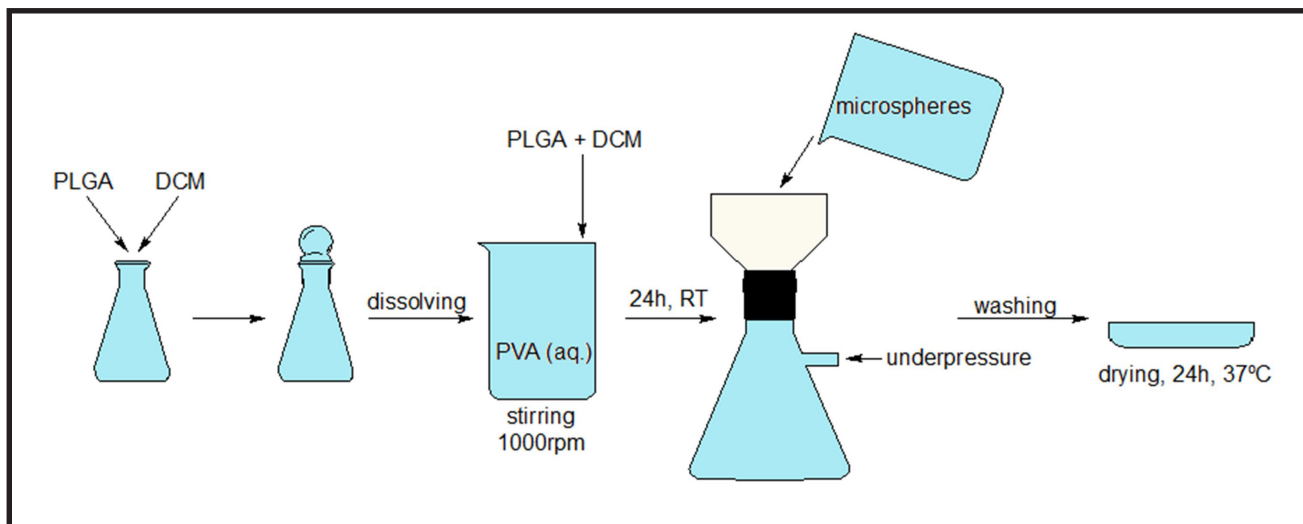


FIG. 1. Scheme of PLGA MS manufacturing by oil-in-water emulsification.

Methods

MS manufacturing by oil-in-water method

To obtain MS, the oil-in-water emulsification was used (FIG. 1). The required amount of PLGA was weighed on an electronic laboratory balance. Under a fume hood, a propeller was put in a glass bottle, then DCM was poured. A ground glass stopper was put to prevent the DCM evaporation. The bottle was placed on a magnetic stirrer and it was turned on to make the propeller rotate. Subsequently, PLGA was added. Such a sequence prevented the polymer particles sticking to the propeller or the glass bottle and assured the PLGA proper dissolution. The glass stopper was inserted into the bottle neck promptly and protected with Parafilm to diminish the DCM evaporation, which would adversely change the ultimate PLGA concentration. The applied oil phase was the PLGA in DCM solution at the 5-10% concentration range.

The water phase was prepared by dissolving PVA in water to obtain the 4% solution. Similarly, the beaker with the propeller was prepared, PVA weighed, a small amount of water added and the stirring started. PVA was added, then the bottle was slowly filled with water to avoid sticking PVA to the bottle walls or the propeller. The bottle was left overnight and then the obtained solution was filtered with a filter paper to remove trace amounts of undissolved PVA. The obtained solution was stored at 4°C in the capped bottle additionally protected with Parafilm and then used as a concentrated stock solution, due to its longer time of preparation as compared to the oil phase. Prior to every synthesis, an exact amount of the PVA solution was diluted to the desired concentration (0.1-4%). The 50 ml water phase was poured into the 100 ml beaker. The process was performed at room temperature.

For the MS synthesis, the beaker containing the water phase was placed on the magnetic stirrer (JeioTech, Model MS-52M) and the propeller was added. While adding the oil phase (always 1 ml with an automatic pipette and the same type of tip) near the beaker wall, the water phase was stirred (at a defined speed of 100-2000 rpm). Placing the oil phase precisely on the beaker wall or in the beaker center resulted in a very low MS production efficiency and a high number of inhomogeneous particles or fibrous structures. The MS were left overnight to solidify via the DCM evaporation. Subsequently, they were vacuum filtered and washed with distilled water multiple times to ensure the PVA residues removal. Then the MS were moved to a Petri dish and left to dry at 37°C for 24 h.

MS sieving and cleaning

In order to obtain MS free of defects such as fibers or foils and endowed with the defined and coherent diameters, the additional process of sieving and cleaning was required. Furthermore, some MS revealed air bubbles entrapped inside, which made them float on the water surface or the cell culture medium. This behavior is highly disadvantageous regarding the culture conditions of bone cells which need a support to adhere and grow. That is why the dried MS were sieved using a grid of 200 μm to collect the MS of higher diameters. Subsequently, the MS fraction was added to a beaker with distilled water, stirred manually, and left for 5 min. After that, the MS which sank to the beaker bottom were collected with a 10 ml pipette. Finally, the MS were dried and stored at 4°C for further studies.

Determining the MS microstructure and size

The MS were observed with an optical digital microscope Keyence VHX-900F. For each sample batch, the diameter of 600 individual MS was measured with the device software and Fiji (ImageJ) software. The data was analyzed by the Shapiro-Wilk test (Origin Pro 2020 9.7.0.188 Academic) to check normality. Since the distribution failed the Shapiro-Wilk test, the results were displayed as histograms and the median was calculated.

Results and Discussion

To obtain MS with the desired average diameter and diameter distribution suitable for bone MTE, three parameters were examined: the stirring speed of the water phase during MS manufacturing, the surfactant concentration, i.e. PVA in the water phase, and the PLGA concentration in the oil phase.

Stirring speed

During the oil-in-water emulsification, the stirring speed has a significant impact on the shear of oil phase flux and on the MS diameter. In this experiment, the PLGA/DCM solution ratio was set at 7.5% and the PVA concentration at 1%, while five different stirring speeds of the water phase were tested: 100 rpm, 250 rpm, 500 rpm, 1000 rpm and 2000 rpm. It was found that the 100 rpm stirring speed was too low to form MS – only fibers and irregular foils were obtained. The results showed that all the MS were transparent and exhibited a smooth appearance (FIG. 2, left column).

The results presented in histograms (FIG. 2, right column) showed that for the steering speed of 250 and 500 rpm the MS sizes were similar but the size distribution changed. The percentage of MS with the diameter over 325 μm dropped from 71.5 to 50.6 and the contribution of MS with lower diameters increased. For the steering speed of 1000 rpm a much higher differences were observed. The shape of histogram changed, and the percentage of 115 and 175 μm MS equaled 39%. The highest stirring speed of 2000 rpm resulted in even a higher percentage of MS with the low diameter. The MS of 175 μm or below in diameter represented 72.2% of all the formed MS. Thus, for further studies, the steering speed of 1000 rpm was selected.

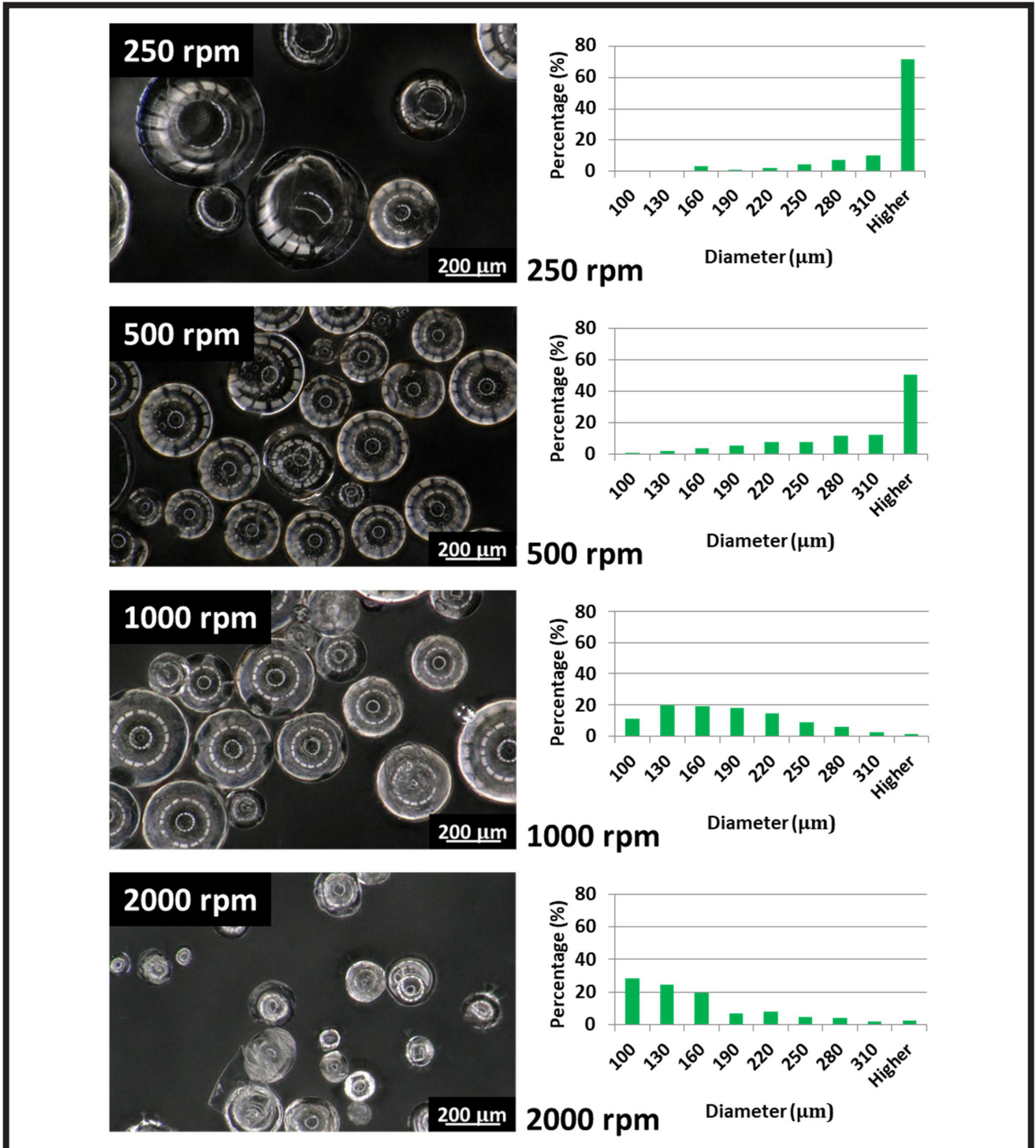


FIG. 2. Optical microscopy pictures (left column) and diameter distribution histograms of PLGA microspheres (right column) obtained at a different stirring speed of water phase (250, 500, 1000 and 2000 rpm); with constant other parameters: PLGA = 7.5%, PVA = 1%; histograms prepared based on $n = 600$ MS.

PVA concentration in water phase

In this experiment five concentrations of PVA in the water phase were examined: 0.1%, 0.5%, 1%, 2% and 4%. The PLGA concentration in the DCM oil phase was 7.5% and the stirring speed – 1000 rpm. The MS morphology, size and size distribution were analyzed and compared. The results of the MS morphology observed under an optical microscope and the corresponding size distribution values are shown in FIG. 3. The results proved all the MS to be transparent and endowed with a smooth appearance (FIG. 3, left column).

The histograms presented in FIG. 3, right column, show that the percentage of the biggest MS (>260 μm) was the highest (44.4%) for the MS produced at the 0.1% PVA concentration. For the higher PVA concentrations (0.5%, 1% and 2%) no significant trend in distribution was observed – a wide variety of diameters in the samples was measured. For the 4% PVA, as expected, the highest number of MS (26.8%) was in the lowest partition of 70 μm and in every next partition it steadily decreased. According to the obtained results, the PVA concentration in the water phase of 0.5-2% was suitable to produce MS. Thus, the 1% PVA was used to manufacture MS in further studies.

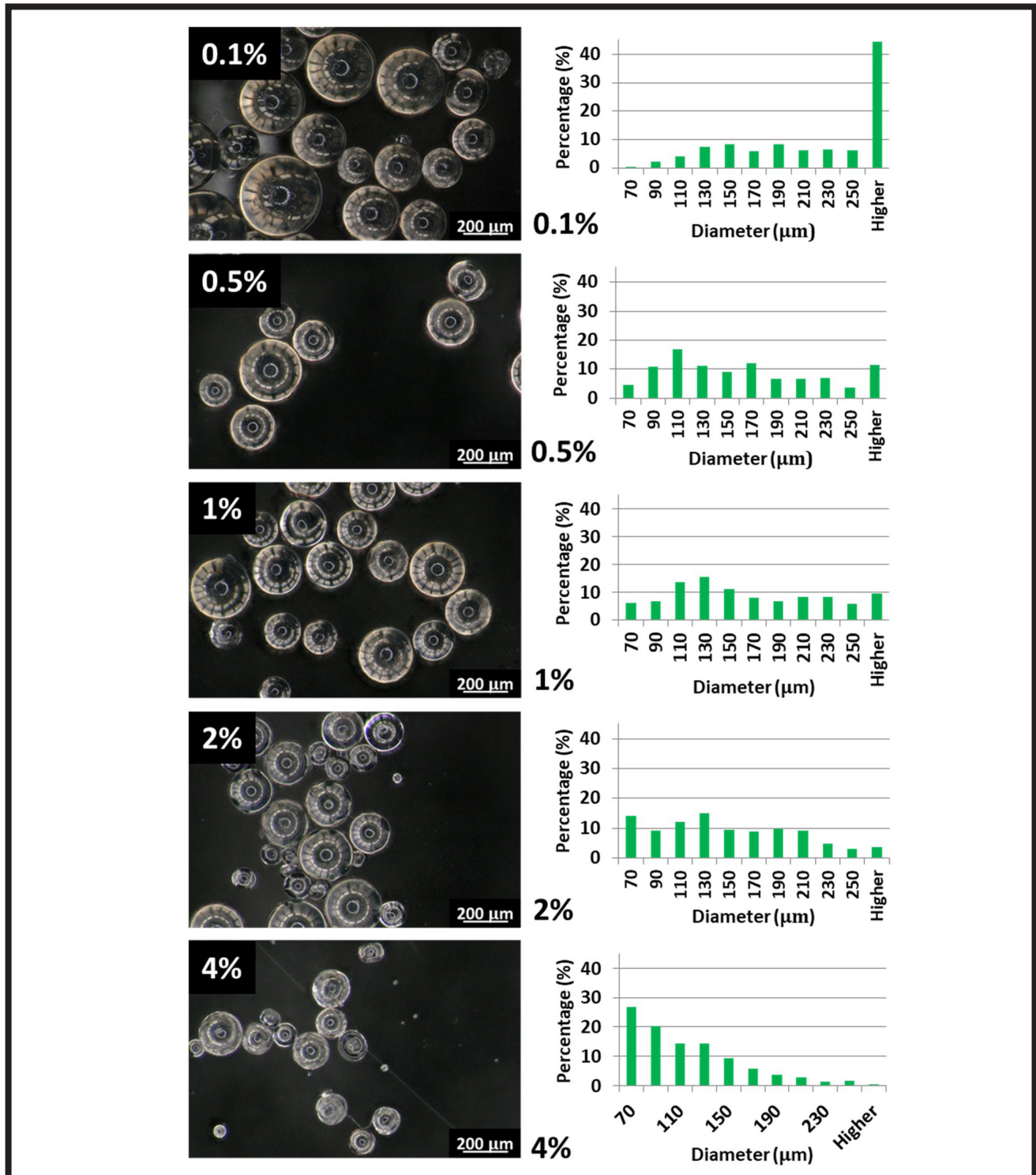


FIG. 3. Optical microscopy pictures (left column) and diameter distribution histograms of PLGA microspheres (right column) obtained at different PVA concentrations in water phase (0.1%, 0.5%, 1%, 2% and 4%); with constant other parameters: PLGA = 7.5%, stirring speed = 1000 rpm; histograms prepared based on n = 600 MS.

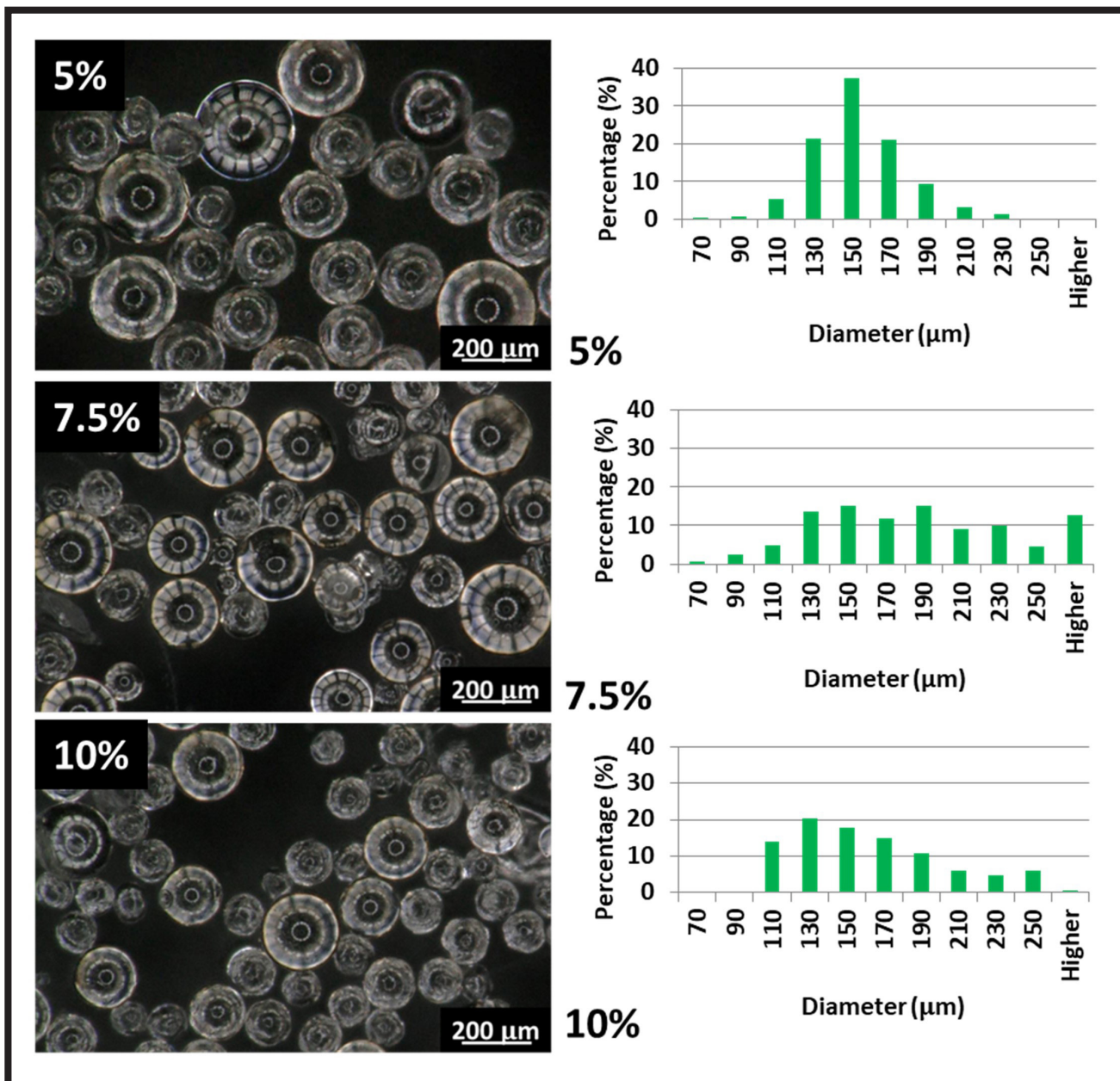


FIG. 4. Optical microscopy pictures (left column) and histograms of diameter distribution of PLGA microspheres (right column) obtained at different concentrations of PLGA in oil phase (5%, 7.5% or 10%); with constant other parameters: 1000 rpm, PVA = 1%); histograms prepared based on $n = 600$ MS.

PLGA concentration in oil phase

In this experiment three concentrations of PLGA in DCM solution (5%, 7.5% and 10%) were examined and their impact on the MS morphology, size and size distribution was analyzed and compared. In this case, the stirring speed and the PVA concentration were constant (1000 rpm and 1%, respectively). The results showing morphology of the MS observed under an optical microscope and the corresponding size distribution values are shown in FIG. 4. The results showed that all the MS were transparent and exhibited a smooth appearance.

The samples produced from the 5% PLGA concentration in the oil phase revealed the narrowest MS diameter distribution. The highest percentage (37.4%) had the size of 140-160 μm and almost 80% of all the MS obtained at this PLGA concentration fell in the range of 120 μm and 180 μm . However, the obtained data did not show normal distribution (normality checked according to the Shapiro-Wilk test).

The MS diameter distribution was the most irregular at the 7.5% PLGA concentration in the oil phase. These were the only conditions where 12.6% of MS had the diameter higher than 260 μm and for almost 3% of MS the diameter was lower than 100 μm . The MS diameter distribution was more regular for the 10% PLGA concentration than for the 7.5% PLGA in the oil phase. The highest percentage of microspheres (20%) had the size of 120-140 μm . The percentage of MS with higher diameters decreased, for instance less than 1% of all the MS had the diameter higher than 260 μm .

According to the obtained data, the 7.5% PLGA concentration in the oil phase was considered optimal for the MS manufacturing.

Comparison of median MS diameters

In order to visualize and compare the obtained results, median diameters of MS manufactured under different conditions were collected and presented in FIG. 5.

The results shown in FIG. 5A revealed a strong dependence between the stirring speed and the mean MS diameter – namely, the higher the stirring speed, the lower diameter. At the lowest speed (250 rpm) the median diameter was the highest (383.0 μm) and it decreased slightly (to 312.0 μm) when the speed was doubled. The twofold increase in speed (to 1000 rpm) resulted in almost two-time lower median MS diameter (161.5 μm). The further speed increase did not have a considerable impact on the MS median diameter: the 2000 rpm speed led to the MS with the median diameter of 144 μm .

The results presenting the MS median diameter produced at five concentrations of PVA in the water phase (0.1%, 0.5%, 1%, 2% and 4%) are presented in FIG. 5B. The results showed that the PVA concentration significantly influenced the MS diameter: the higher concentration, the lower diameter. The highest median diameter for 0.1% PVA was 323 μm , and the lowest for PVA 4% was 94 μm , so the MS diameter changed more than twice. Therefore, the PVA concentration may be considered a very convenient and effective factor to control the MS diameter.

The results presenting the MS median diameter produced at three concentrations of PLGA in DCM solution (5%, 7.5% and 10%) are presented in FIG. 5C. The results showed that the PLGA concentration in the oil phase did not have a significant impact on the MS median diameter.

In order to perform statistical analysis, we took into account all the data regarding the diameters of 1,800 individual MS. The reason behind such an approach was the fact that the manufacturing conditions shown in FIG. 2 (for the stirring speed of 1000 rpm), FIG. 3 (for 1% PVA) and FIG. 4 (for 7.5% PLGA concentration) were the same and corresponded to the samples obtained at the following parameters: 7.5% PLGA, 1% PVA, 1000 rpm. First, the Shapiro-Wilk analysis revealed that the collected data was not of normal distribution so we presented it as a histogram (FIG. 6). The size distribution proved that the highest number of MS (67.5%) was in the range between 115 and 235 μm . The median diameter of MS equaled 159.4 μm , which almost perfectly fit the expected diameter of 160 μm .

PLGA MS sieving and cleaning process

The optical microscopy pictures and histograms of the PLGA MS diameter distribution before and after the sieving and cleaning processes are presented in FIG. 7. The results showed that MS with more homogenous diameters and diameter distribution were successfully selected thanks to the developed procedure. The sieving and cleaning process effectively increased the MS content with the mean diameter of 280 μm and the MS distribution became more homogenous.

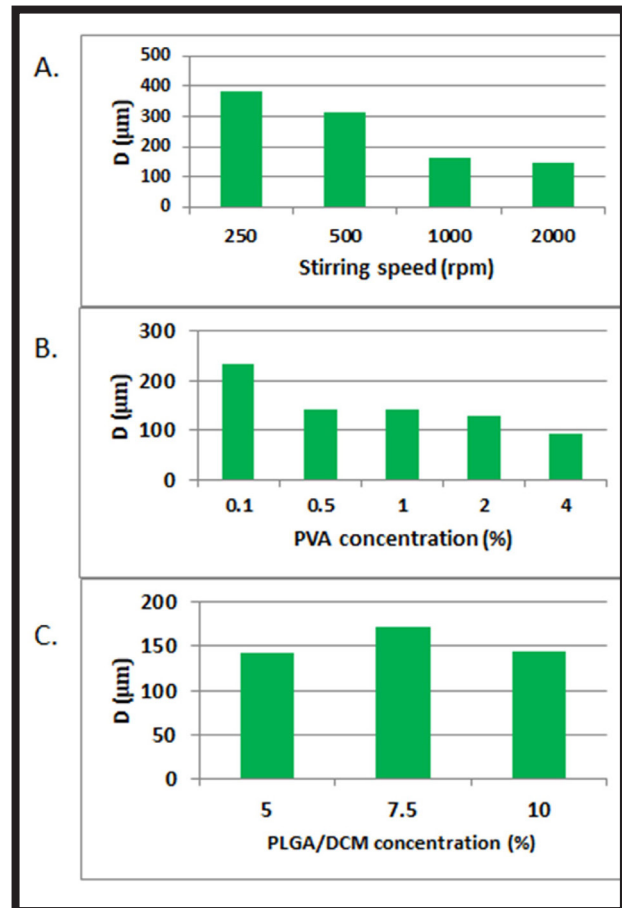


FIG. 5. Median diameter (D) of PLGA microspheres: (A) obtained with a different stirring speed of water phase (250, 500, 1000, 2000 rpm), for constant PLGA concentration of 7.5%, and PVA concentration of 1%; (B) obtained for different concentration of PVA in water phase (0.1%, 0.5%, 1%, 2% and 4%), for constant PLGA concentration of 7.5% and stirring speed in water phase of 1000 rpm; and (C) obtained at different concentration of PLGA in oil phase (5%, 7.5% or 10%); for constant steering speed of 1000 rpm and PVA concentration of 1%; diameter measured for $n = 600$ individual MS for each manufacturing condition.

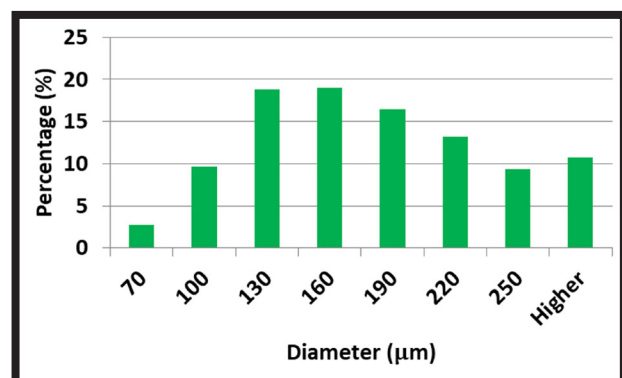


FIG. 6. Histogram of diameter distribution of PLGA microspheres obtained at 7.5% PLGA/DCM concentration in oil phase, 1% PVA concentration in water phase and 1000 rpm stirring speed of water phase; histogram prepared based on $n = 1800$ MS.

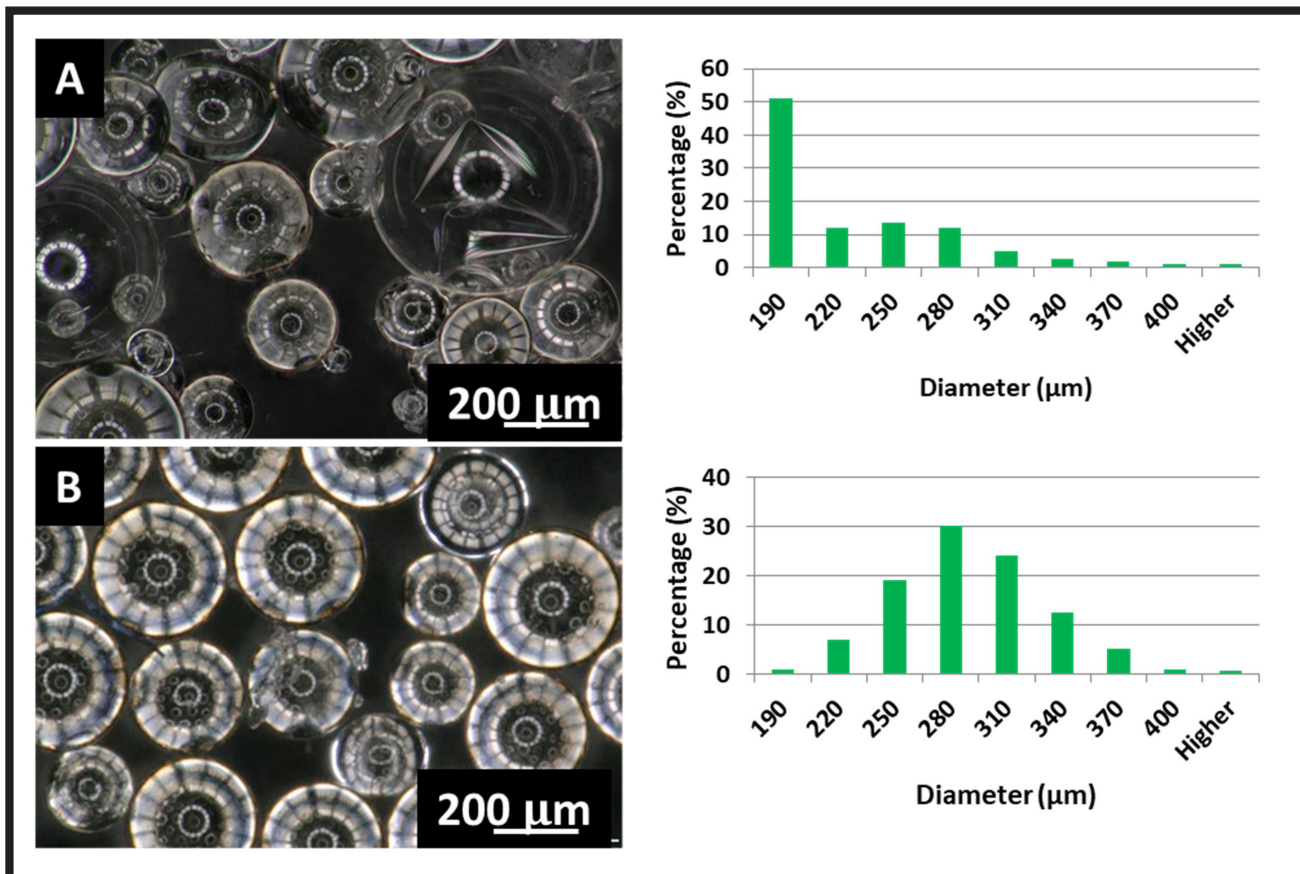


FIG. 7. Optical microscopy pictures (left column) and histograms of diameter distribution of PLGA microspheres (right column) before (A) and after sieving and cleaning process (B) (left column); PLGA concentration in oil phase 7.5%, PVA concentration in water phase 1%, stirring speed 1000 rpm; diameter measured for $n = 600$ individual MS for each manufacturing condition.

Conclusion

Three parameters – the stirring speed of the water phase, the PVA concentration in the water phase and the PLGA concentration in the oil phase – and their impact on the MS mean diameter and its distribution were examined. The most significant changes were observed for the PVA concentration and the stirring speed – the higher concentration or stirring speed, the lower MS diameter, which was consistent with the literature findings [6].

The aim of our experiments was to obtain MS that could be used for MTE cell cultures and to create cell-tissue constructs. The diameter distribution is of key importance in such an application – the higher variety of diameters is expected to create more complex and irregular constructs. On the other hand, the lower diameter range may be favorable for different applications where high repeatability is desired (e.g. 3D printing with MS used as cell carriers). For all the examined parameters the highest variety of diameters was observed for average values of the investigated PVA concentration in the water phase, the PLGA concentration in the oil phase, and the average values of the stirring speed.

Taking into consideration all the criteria to choose the parameters and the mean diameter, which according to literature should equal 100-300 μm , the optimal manufacturing parameters turned out to be: the 7.5% PLGA concentration in DCM solution as the oil phase, the 1-2% concentration of PVA solution as the water phase and the 1000 rpm stirring speed of the water phase. This combination of parameters guaranteed the MS mean diameter equal to 160 μm .

It was found that due to the MS sieving and cleaning process the MS with more narrow size distribution was successfully obtained. Moreover, only the MS endowed with the mean diameter of 280 μm sank in the cell culture medium and were collected from the cell culture wells bottoms.

All the aforementioned properties are highly advantageous with regard to cell culturing and modular bone tissue engineering applications.

Acknowledgements

This study was supported by National Science Center, Poland (Grant No. UMO-2016/21/D/ST8/0185), by the Program "Excellence Initiative – Research Universtity" for the AGH University of Science and Technology and by the Faculty of Materials Science and Ceramics, AGH – UST (Subsidy No. 16.16.160.557).

ORCID iDs

B. Mielan:
E. Pamula:

<https://orcid.org/0000-0002-1226-3540>
<https://orcid.org/0000-0002-0464-6189>

References

- [1] H. Onoe, S. Takeuchi: Cell-laden microfibers for bottom-up tissue engineering. *Drug Discov. Today*. 2 (2014) 236–246. <https://doi.org/10.1016/j.drudis.2014.10.018>.
- [2] J.W. Nichol, A. Khademhosseini: Modular tissue engineering: engineering biological tissues from the bottom up. *Soft Matter*. 5 (2010) 1312–1319. <https://doi.org/10.1039/b814285h>.
- [3] C.R. Correia, S. Nadine, J.F. Mano: Cell Encapsulation Systems Toward Modular Tissue Regeneration: From Immunoisolation to Multifunctional Devices, *Adv. Funct. Mater.* 1908061 (2020) 1–23. <https://doi.org/10.1002/adfm.201908061>.
- [4] C.A. Custódio, V.E. Santo, M.B. Oliveira, M.E. Gomes, R.L. Reis, J.F. Mano: Functionalized Microparticles Producing Scaffolds in Combination with Cells. *Adv. Funct. Mater.* 24 (2014) 1391–1400. <https://doi.org/10.1002/adfm.201301516>.
- [5] C.J. Connon: Approaches to Corneal Tissue Engineering: Top-down or Bottom-up? *Procedia Eng.* 110 (2015) 15–20. <https://doi.org/10.1016/j.proeng.2015.07.004>.
- [6] T. Kemala: Preparation and characterization of microspheres based on blend of poly (lactic acid) and poly (ε-caprolactone) with poly(vinyl alcohol) as emulsifier. *Arab. J. Chem.* 5 (2012) 103–108. <https://doi.org/10.1016/j.arabjc.2010.08.003>.
- [7] B. Li, X. Wang, Y. Wang, W. Gou, X. Yuan, J. Peng, Q. Guo, S. Lu: Past, present, and future of microcarrier-based tissue engineering. *J. Orthop. Transl.* 3 (2015) 51–57. <https://doi.org/10.1016/j.jot.2015.02.003>.
- [8] Shu-ying Wang, Xu-dong Shi, Zhi-hua Gan, Feng Wang: Preparation of PLGA Microspheres with Different Porous Morphologies. *Chinese J. Polym. Sci.* 33(1) (2015) 128-136. doi: 10.1007/s10118-014-1507-9
- [9] C. Fu, X. Yang, S. Tan, L. Song: Enhancing Cell Proliferation and Osteogenic Differentiation of MC3T3-E1 Pre-osteoblasts by BMP-2 Delivery in Graphene Oxide-Incorporated PLGA/ HA Biodegradable Microcarriers. *Sci. Rep.* 7 (2017) 1–13. <https://doi.org/10.1038/s41598-017-12935-x>.
- [10] S. Yu, S. Yao, Y. Wen, Y. Wang, H. Wang, Q. Xu: Angiogenic microspheres promote neural regeneration and motor function recovery after spinal cord injury in rats. *Nat. Publ. Gr.* 6 (2016) 1–13. <https://doi.org/10.1038/srep33428>.
- [11] F. Ito, H. Fujimori, K. Makino: Incorporation of water-soluble drugs in PLGA microspheres. *Colloids Surfaces B Biointerfaces.* 54 (2007) 173–178. <https://doi.org/10.1016/j.colsurfb.2006.10.019>.
- [12] R.H. Parikh, J.R. Parikh, R.R. Dubey, H.N. Soni, K.N. Kapadia, Poly (D, L-Lactide-Co-Glycolide) Microspheres Containing 5-Fluorouracil: Optimization of Process Parameters, *AAPS Pharm Sci Tech.* 4 (2003) 1–8.

EVALUATION OF THE STRENGTH PROPERTIES OF MATERIALS INTENDED FOR TRACHEOBRONCHIAL TUBES

ROBERT SOBOTA^{1*}, JAROSŁAW MARKOWSKI¹,
KAMIL JOSZKO², BOŻENA GZIK-ZROSKA³,
EDYTA KAWLEWSKA², MAREK GZIK²

¹ CLINICAL DEPARTMENT OF LARYNGOLOGY,
MEDICAL UNIVERSITY OF SILESIA,
20-24 FRANCUSKA STR., KATOWICE, POLAND

² DEPARTMENT OF BIOMECHATRONICS,
SILESIA UNIVERSITY OF TECHNOLOGY,
40 ROOSEVELTA STR., ZABRZE, POLAND

³ DEPARTMENT OF BIOMATERIALS AND MEDICAL DEVICES
ENGINEERING, SILESIA UNIVERSITY OF TECHNOLOGY,
40 ROOSEVELTA STR., ZABRZE, POLAND

*E-MAIL: ROBERTSOBOTA85@GMAIL.COM

Abstract

The desire to increase the comfort of patients and to continue production despite the decreasing amount of available materials on the market has led to the constant search for novel materials that could be used to obtain tracheobronchial tubes. The aim of this study is to determine the mechanical properties of a new thermoplastic elastomer. Two materials - the thermoplastic elastomer and the natural rubber were subjected to three tests: static tensile test, static compression test and static three-point bending test. During the static tensile test, samples of the tested materials were examined, and during the next two examinations, the final products. The materials underwent the processes of sterilization, hydrolytic degradation and degradation by oxidation. The treated samples were also tested in order to compare the obtained results.

The mechanical properties of the tested materials improved both after the hydrolytic degradation and oxidative degradation, as well as after the sterilization process. Yet the thermoplastic elastomer revealed a more noticeable increase. The elastomer hardening is a positive phenomenon potentially leading to fewer accidental closures of the tubes cross-section. Both the sterilization process and various degradation methods improved the mechanical properties by strengthening the tested materials. This phenomenon seems to be desirable to avoid the closure of the implemented tube during its application.

Keywords: thermoplastic elastomer, tracheobronchial tubes, oxidative degradation, hydrolytic degradation

[*Engineering of Biomaterials* 156 (2020) 10-16]

doi:10.34821/eng.biomat.156.2020.10-16

Introduction

Both T-type endotracheal tubes and Y-type tracheobronchial tubes are used to allow patients to breathe freely in cases of stenosis or obstruction of the airway lumen as a consequence of e.g. cancer or trauma. Endotracheal tubes additionally support the larynx and trachea tissues during the reconstruction of these organs, not only providing natural airway through the upper respiratory tract but also bypassing breathing through the tracheostomy. The main function of tracheobronchial tubes is to restore the trachea and main bronchi patency [1-3].

As any medical device inserted inside the human body, both types of tubes may cause side effects, such as infection and bleeding in the respiratory organs, shortness of breath and inflammation. There is also a possibility of stent displacement. In order to minimize the likelihood of such adverse effects, the tubes must be properly implanted by qualified medical personnel. At the same time, these devices should be made of a suitable material that does not cause severe or chronic reactions and is characterized by high bio-tolerance and appropriate strength properties [3-6].

So far, endotracheal and tracheobronchial tubes have been made of natural rubber but its availability on the market is constantly decreasing. The need to maintain tubes production and help patients made scientists search for innovative, more cost-effective and convenient solutions. Thermoplastic elastomers are widely used for medical applications and can be processed using a variety of manufacturing technologies. The use of this material has the potential to increase the production of tracheobronchial tubes and to reduce the cost per part, compared to the currently used material [7-9].

Thermoplastic elastomers are composite elastomeric materials showing the features typical for elastomers at normal use temperatures and thermoplastic resins at elevated temperatures, and their production is based on methods for generating thermo-reversible nodes of a spatial network. Such a network is made up of soft elastomeric phases separated at the nanoscale level and crystalline or amorphous phases [10-12].

Considering the described problems, the aim of this study is to determine the mechanical properties of new material - a thermoplastic elastomer used in the production of tracheobronchial tubes.

Materials and Methods

The research was carried out in two stages at the Faculty of Biomedical Engineering of the Silesian University of Technology. The first stage was to test the samples cut from tracheostomy tubes made of two materials: the thermoplastic elastomer and natural rubber. In order to perform the cutting procedure correctly, a special handle was prepared, using the 3D printing technology. The dimensions of the resulting samples are shown in FIG. 1.

The obtained samples were divided into five groups:

- sterilized samples,
- samples sterilized and subjected to the process of hydrolytic degradation lasting 60 days,
- samples sterilized and subjected to the process of hydrolytic degradation lasting 2 days,
- samples sterilized and subjected to the process of oxidative degradation lasting 60 days,
- samples sterilized and subjected to the process of oxidative degradation lasting 2 days.

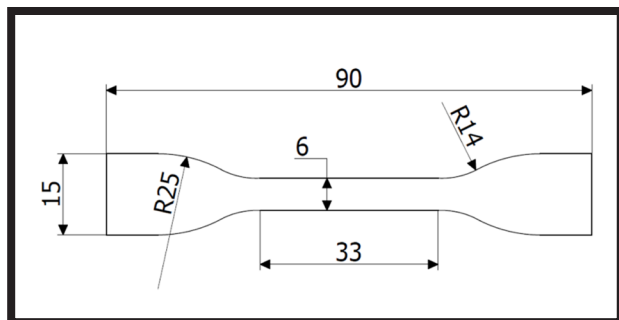


FIG. 1. Dimensions of tested samples.

Hydrolytic degradation and oxidative degradation were performed in accordance to the standard PN-EN ISO:10993-13:2010 („Biological evaluation of medical devices – Part 13: Identification and quantification of degradation products from polymeric medical devices”). The factor of hydrolytic degradation was distilled water and for oxidative degradation – 3% hydrogen peroxide of pharmacological pureness (replaced daily). The specimens were stored in glass. A heat chamber Venticell 111 was used. The test was performed using the accelerated method at the temperature of 70°C +/- 2°C for two periods of time: 2 days and 60 days.

The sterilization process was carried out under the same conditions as for all medical products and accessories. The samples were sterilized with ethylene oxide (10% of C₂H₄O and 90% of CO₂) for minimum 3 hours. The sterilization temperature was 53°C +/- 5°C, the pressure 2.5 bar +/- 5%.

Each group contained 10 samples: 5 made of thermoplastic elastomer and 5 made of natural rubber. The total was 50 samples. The samples were subjected to the static tensile test at a speed of 20 mm/min, using the static testing machine MTS Criterion Model 43. The following properties were determined on the basis of the performed measurements:

- maximum force F [N],
- Young's modulus [MPa],
- ultimate tensile strength R_m [MPa],
- maximum deformation [mm/mm],
- dimension of sample at the measuring site [mm].

Each tested sample was fixed in the holder so that the measuring distances had the same length for every sample. The results were obtained with accuracy to 1 N. The samples after the hydrolytic and oxidative degradation processes were prepared according to the standard PN-EN ISO:10993-12:2010 („Biological evaluation of medical devices – Part 12: Sample preparation and reference materials”). In the second stage, two tests were carried out on the final products made of natural rubber and the thermoplastic elastomer. Each examination was performed twice, the second time 30 days after the oxidative degradation. The results revealed how the following properties of the tested material changed:

- maximum bending force [N],
- maximum tension [MPa],
- Young's modulus [MPa].

A total of 78 laboratory tests were performed.

The static compression test was performed at a speed of 5 mm/min with the cross-section of the tracheobronchial tube closed at a distance of 20 mm and 85 mm from the tube edge. The measuring distances are shown in FIG. 2.

The static three-point bending test consisted in placing the tube on two supports spaced 50 mm apart and applying the load perpendicular to the longitudinal axis of the product. The supports and the loading element were three cylinders with a diameter of 3 mm. The load was applied at a speed of 5 mm/min.

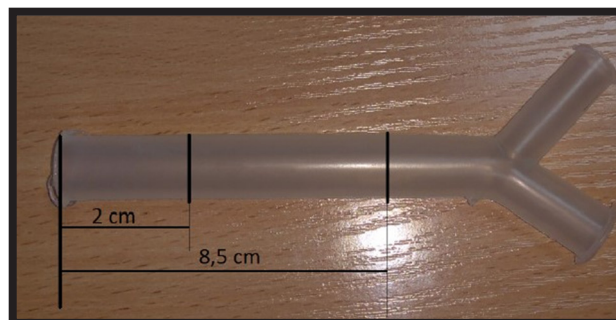


FIG. 2. Measuring distances for static compression test.

Results and Discussion

The results of the static tensile tests for the analyzed non-degraded samples are presented in TABLE 1.

The conducted tests revealed that the samples of natural rubber had lower stiffness than those of the thermoplastic elastomer, which was evidenced by the maximum deformation values. Natural rubber had an average value of 4.41 [mm/mm], while the average deformation for the thermoplastic elastomer was 1.6 [mm/mm]. Moreover, a significant difference in Young's modulus was noticed. For the natural rubber samples, the average value was 2 MPa, while for the thermoplastic elastomer samples it was 15 MPa.

The second static tensile tests were performed after the hydrolytic degradation processes lasting for 2 and 60 days. The results concerning the 2-day process are presented in TABLE 2, while those obtained after 60 days are shown in TABLE 3.

Subsequent static tensile tests were performed on the samples subjected to the oxidative degradation process lasting respectively 2 and 60 days. The obtained results are presented in TABLES 4 and 5.

The graphs presented below show how the values of the three most important criteria - Young's modulus, maximum strength and maximum deformation changed for the samples made of natural rubber and the thermoplastic elastomer subjected to various degradation processes (FIGs. 3-5).

The tests on the final products were carried out on the sterilized and unsterilized samples after the 30-day degradation by oxidation process (30 days is the maximum implant placement time in the body). In each case, the samples of two lengths were observed: 85 mm and 20 mm. The obtained results are presented in TABLES 6-7.

The last static three-point bending test was carried out on the samples prepared in the same way as for the static compression test. The results of that study are presented in TABLES 8-9.

The conducted static tensile tests proved that both the hydrolytic and oxidative degradation processes altered the strength properties of the tested materials. For natural rubber, as a result of hydrolytic degradation, the value of maximum breaking strength increased by 17.5% after 2 days and by 20% after 60 days, when compared to the samples subjected to sterilization only. As a result of degradation by oxidation, the value of maximum breaking strength increased by 23% after 2 days and by 17.7% after 60 days. The same tendency was noticed when determining the ultimate tensile strength. In the case of hydrolytic degradation, the maximum tension increased by 4% after 2 days and by 11.9% after 60 days. In the case of degradation by oxidation, it increased respectively by 11.1% and 8.1%.

TABLE 1. Static tensile test results for samples made of natural rubber (marked as K) and thermoplastic elastomer (marked as E).

Number of sample	Young modulus [MPa]	Ultimate tensile strength R_m [MPa]	Maximum force F [N]	Maximum deformation [mm/mm]	Thickness [mm]	Width [mm]
K1	2	6.4	65	4.101	1.7	6
K2	2	7.9	81	4.498	1.7	6
K3	2	8.4	74	4.532	1.6	5.5
K4	2	8.8	84	5.525	1.6	6
K5	2	5.3	51	3.404	1.6	6
Average	2	7.36	71	4.41	1.64	5.9
SD	0	1.47	13.36	0.77	0.05	0.22
E1	17	2.9	26	1.544	6	1.5
E2	13	2.2	21	1.229	6	1.6
E3	15	2.5	24	1.679	6.2	1.55
E4	15	2.7	26	1.557	6	1.65
E5	15	2.9	28	1.989	6	1.6
Average	15	2.64	25	1.5996	6.04	1.58
SD	1.41	0.30	2.65	0.27	0.09	0.06

TABLE 2. Static tensile test results for samples made of natural rubber (K) and thermoplastic elastomer (E) after the 2-day hydrolytic degradation.

Number of sample	Young modulus [MPa]	Ultimate tensile strength R_m [MPa]	Maximum force F [N]	Maximum deformation [mm/mm]	Thickness [mm]	Width [mm]
K11	2	7.3	88	4.842	2	6
K12	2	6.7	71	4.435	1.7	6.2
K13	2	7.6	86	4.597	1.9	6
K14	2	6.8	74	4.235	1.8	6
K15	2	9.9	98	5.043	1.7	5.8
Average	2	7.66	83.4	4.6304	1.82	6
SD	0.0	1.30	11.0	0.32	0.13	0.14
E11	16	2.6	29	1.636	1.8	6.1
E12	17	2.9	27	1.554	1.6	5.9
E13	15	2.7	31	1.326	1.7	6.88
E14	14	2.9	29	1.745	1.7	6
E15	18	2.6	26	1.135	1.6	6.2
Average	16	2.74	28.4	1.4792	1.68	6.2
SD	1.6	0.15	1.9	0.25	0.08	0.39

TABLE 3. Static tensile test results for samples of natural rubber (K) and thermoplastic elastomer (E) after the 60-day hydrolytic degradation.

Number of sample	Young modulus [MPa]	Ultimate tensile strength R_m [MPa]	Maximum force F [N]	Maximum deformation [mm/mm]	Thickness [mm]	Width [mm]
K6	2	6.9	73	5.042	1.8	5.9
K7	2	8.5	92	5.251	1.7	6.4
K8	2	7.7	73	4.536	1.6	5.9
K9	2	8.4	91	5.433	1.9	5.7
K10	2	9.7	97	5.52	1.7	5.9
Average	2	8.24	85.2	5.154	1.74	5.96
SD	0.0	1.04	11.4	0.39	0.11	0.26
E6	13	3.1	0.032	1.647	6.45	1.6
E7	18	2.8	0.026	1.643	5.7	1.6
E8	14	2.6	0.028	1.555	6.5	1.6
E9	17	2.7	0.024	1.506	5.7	1.55
E10	16	2.9	0.03	1.48	6.1	1.7
Average	15.6	2.82	0.028	1.5662	6.09	1.61
SD	2.1	0.19	0.0	0.08	0.39	0.05

TABLE 4. Static tensile test results for samples of natural rubber (K) and thermoplastic elastomer E after the 2-day oxidative degradation.

Number of sample	Young modulus [MPa]	Ultimate tensile strength R_m [MPa]	Maximum force F [N]	Maximum deformation [mm/mm]	Thickness [mm]	Width [mm]
K21	2	9	90	5.482	1.7	5.9
K22	2	8.9	97	5.12	1.8	6.1
K23	2	8.1	83	4.685	1.7	6
K24	2	6.7	73	4.077	1.8	6
K25	2	8.2	94	5.039	1.9	6
Average	2	8.18	87.4	4.8806	1.78	6
SD	0.0	0.92	9.6	0.53	0.08	0.07
E21	16	3	29	1.683	1.6	6
E22	19	3.4	34	1.906	1.6	6.2
E23	16	2.8	25	1.575	1.5	6
E24	18	2.8	27	1.26	1.6	6.2
E25	16	2.5	31	1.196	1.9	6.5
Average	17	2.9	29.2	1.524	1.64	6.18
SD	1.4	0.33	3.5	0.30	0.15	0.20

TABLE 5. Static tensile test results for samples of natural rubber (K) and thermoplastic elastomer (E) after the 60-day oxidative degradation.

Number of sample	Young modulus [MPa]	Ultimate tensile strength R_m [MPa]	Maximum force F [N]	Maximum deformation [mm/mm]	Thickness [mm]	Width [mm]
K16	2	6.3	64	4.192	1.8	5.7
K17	2	8.5	10	5.748	1.8	6.5
K18	2	9.8	99	5.477	1.6	6.3
K19	2	8	89	5.585	1.8	6.2
K20	2	7.2	66	4.397	1.6	5.7
Average	2	7.96	83.6	5.0798	1.72	6.08
SD	0.0	1.32	34.5	0.73	0.11	0.36
E16	19	1.8	18	0.343	1.7	5.9
E17	15	1.5	15	0.29	1.6	6.1
E18	17	1.4	15	0.288	1.7	6
E19	16	1.4	16	0.379	1.7	6.5
E20	17	1.2	11	0.253	1.5	6.4
Average	16.8	1.46	15	0.3106	1.64	6.18
SD	1.5	0.22	2.5	0.05	0.09	0.26

TABLE 6. Results of static compression test obtained for thermoplastic elastomer samples.

Type of sample	8.5 cm			2 cm		
	Maximum force F [N]	Maximum tension [MPa]	Young modulus [MPa]	Maximum force F [N]	Maximum tension [MPa]	Young modulus [MPa]
Samples unsterilized	6.66	0.128	1.53	5.96	0.118	1.31
Samples unsterilized, after 30 days of degradation	7.42	0.138	1.86	6.43	0.120	1.47
Samples sterilized	7.33	0.137	1.61	6.35	0.118	1.34
Samples sterilized, after 30 days of degradation	7.66	0.142	1.96	6.75	0.126	1.59

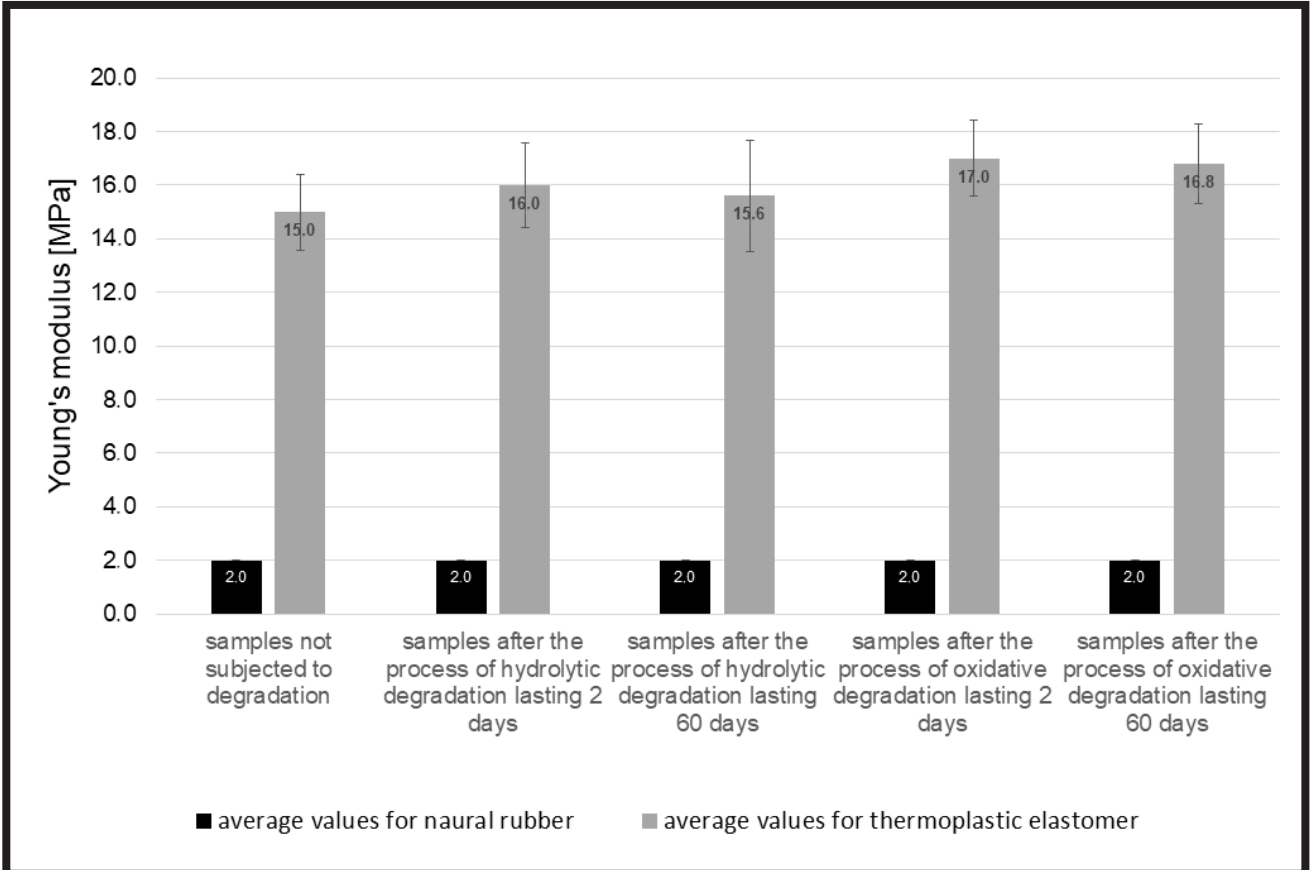


FIG. 3. Values of Young's modulus obtained for the samples subjected to various degradation processes.

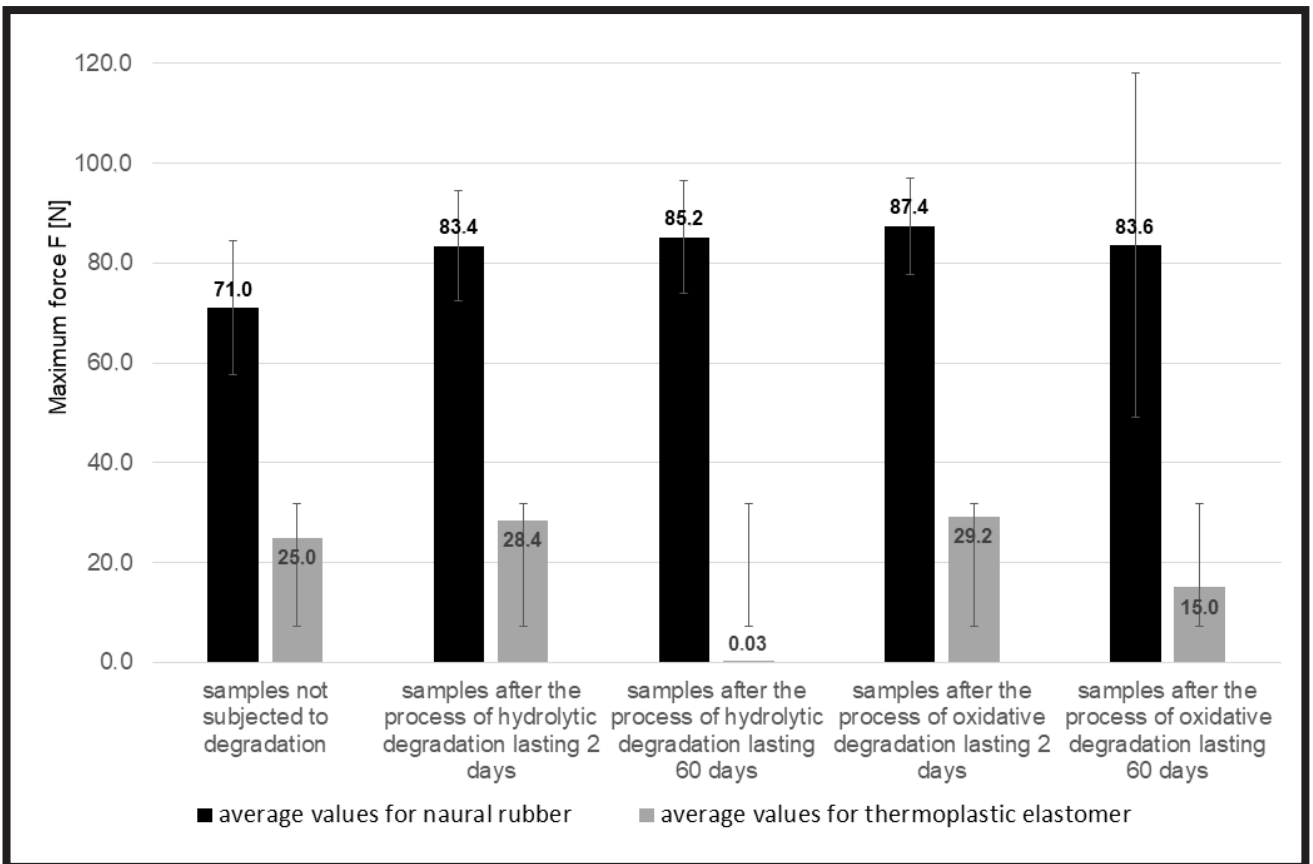


FIG. 4. Values of maximum strength F obtained for the samples subjected to various degradation processes.

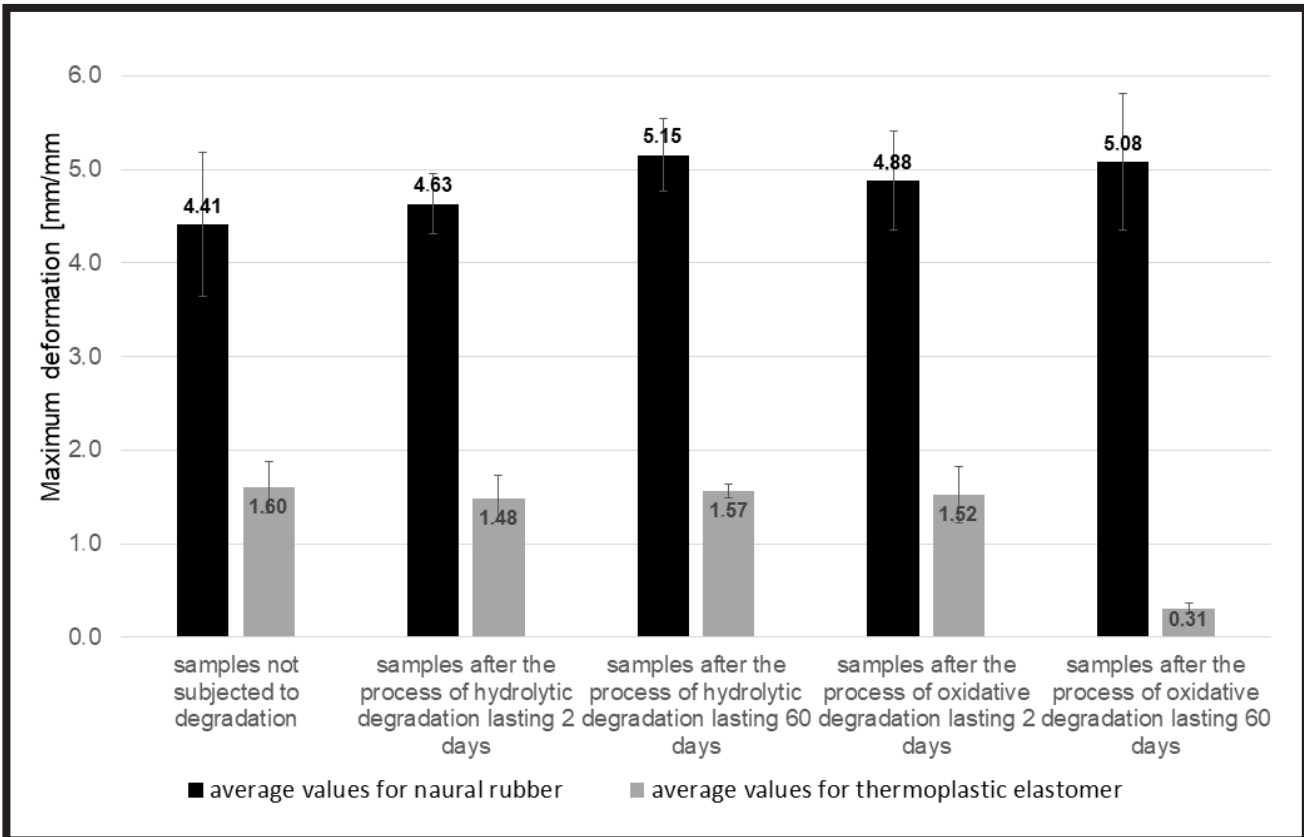


FIG. 5. Values of maximum deformation obtained for the samples subjected to various degradation processes.

TABLE 7. Results of static compression test obtained for natural rubber samples.

Type of sample	8.5 cm			2 cm		
	Maximum force F [N]	Maximum tension [MPa]	Young modulus [MPa]	Maximum force F [N]	Maximum tension [MPa]	Young modulus [MPa]
After sterilization	4.95	0.094	0.86	5.20	0.099	0.96
30 days after sterilization	4.86	0.073	0.76	4.76	0.072	0.73

TABLE 8. Results of three-point bending test obtained for thermoplastic elastomer samples.

Type of sample	Maximum force F [N]	Maximum tension [MPa]	Young modulus [MPa]
Before sterilization	4.2	0.081	1.4
30 days before sterilization	6.96	0.134	1.62
After sterilization	4.5	0.083	1.3
30 days after sterilization	7.08	0.131	1.60

TABLE 9. Results of three-point bending test obtained for natural rubber samples.

Type of sample	Maximum force F [N]	Maximum tension [MPa]	Young modulus [MPa]
After sterilization	3.3	0.063	0.7
30 days after sterilization	5.41	0.102	0.99

The Young's modulus value for all the variants remained unchanged at 2 MPa. For the thermoplastic elastomer it was observed that, as a result of the hydrolytic degradation, the maximum breaking strength value increased by 13.6% after 2 days and by 12% after 60 days. As a result of oxidative degradation, the strength increased by 16.8% after 2 days and decreased by 40% after 60 days. The ultimate tensile strength after the hydrolytic degradation increased by 3.7% after 2 days and by 6.8% after 60 days. The 2-day degradation by oxidation increased the ultimate tensile strength by 9.8%, while the 60-day degradation caused its decrease by 44.6%. Unlike the natural rubber case, the modulus of elasticity of the tested elastomer samples also changed - as a result of the hydrolytic degradation after 2 days its value increased by 6.6% and by 4% after 60 days, while the degradation by oxidation caused the increase by 13.3% and 12%, respectively.

The static compression tests showed that after the oxidative degradation process the strength properties and stiffness of the thermoplastic elastomer tubes improved. The maximum strength the cross-section was closed with, increased after 30 days of degradation for both types of tubes, before (11.4% increase) and after sterilization (4.5% increase), and the maximum tension increased by 7.8% for the tubes before sterilization and by 3.6% after that process.

However, the biggest difference was observed for the longitudinal elasticity modulus. The non-sterilized tube value increased by 21.5%, and the sterilized one by 12.2%. On the other hand, the natural rubber tubes revealed the lowered mechanical properties over time. After 30 days the maximum closing strength decreased by 1.8%, the maximum tension value by 22.3% and Young's modulus by 11.6%.

During the three-point bending test, an increase in the values was observed over time for the tubes made of thermoplastic elastomer and of natural rubber as well.

On the basis of the conducted research, it can be concluded that both the sterilization and the degradation processes improved the mechanical properties of natural rubber and the thermoplastic elastomer. A similar tendency was noticed for polyethylene intended for injection processing whose mechanical properties improved after the processes of hydrolytic and oxidative degradation [4]. Our tests proved that the tested thermoplastic elastomer was characterized by higher strength than natural rubber, which was observed in both stages of the study.

Since the main function of tracheobronchial tubes is to restore the patency of the trachea and main bronchi, the material strengthening will reduce the likelihood of accidental cross-section closure of the implanted tubes. Therefore, taking into account the strength properties, the tested thermoplastic elastomer meets the requirements set for materials used to produce tracheobronchial tubes. It seems that the elastomer properties are advantageous to even a greater extent than the previously used natural rubber, however, further biological evaluation of the tested material is necessary. The authors are also planning to carry out studies on a larger number of samples to perform statistical analysis.

Conclusions

Both the technological aspect and the desire to increase the comfort of patients led to the search for new better solutions in the production of tracheobronchial tubes. The aim of this study was to determine and compare the mechanical properties of the thermoplastic elastomer and the currently used natural rubber. Based on the research, it can be concluded that the desired mechanical properties of both the tested materials improved after the processes of hydrolytic degradation and degradation by oxidation. The properties were also upgraded via the sterilization process, and in the case of the thermoplastic elastomer the increase was more noticeable. The strengthening phenomenon seems to be desirable for endotracheal tube designs, mainly to avoid the accidental closure of the tube cross-section during its application in the body. In order to determine whether the tested material can be used for tracheobronchial tubes, it is necessary to perform biological evaluation of the medical devices.

Acknowledgements

This work is supported by Medical University of Silesia, as part of statutory research no. PCN-1-081/K/0/O.

ORCID iDs

R. Sobota:  <https://orcid.org/0000-0002-2060-929X>
 J. Markowski:  <https://orcid.org/0000-0003-3416-7354>
 K. Jozsko:  <https://orcid.org/0000-0002-8229-3032>
 B. Gzik-Zroska:  <https://orcid.org/0000-0003-4286-001X>
 E. Kawlewska:  <https://orcid.org/0000-0002-9313-0132>
 M. Gzik:  <https://orcid.org/0000-0003-0598-5921>

References

- [1] Warmus J., Gil T., Gocyk W., Ziętkiewicz M., Kuźdzał J.: Laryngeal reconstruction using autologous rib cartilage and T stent – a case report. *Kardiochirurgia i Torakochirurgia Polska* 8(1) (2011) 86-90.
- [2] Gil T., Warmus J., Włodarczyk J., Grochowski Z., Bederski K., Kocoń P., Talar P., Kuźdzał J.: Iatrogenic injuries to the trachea and main bronchi. *Polish Journal of Cardio-Thoracic Surgery* 2 (2016) 113-116.
- [3] Haas C.F., Eakin R.M., Konkle M.A., Blank R.: Endotracheal tubes: old and new. *Respiratory Care* 59(6) (2014) 933-955.
- [4] Sobota R., Jozsko K., Gzik-Zroska B., Markowski J., Kawlewska E.: Ocena właściwości wytrzymałościowych materiałów na rurki tracheostomijne. *Aktualne Problemy Biomechaniki* 18 (2019) 47-53.
- [5] Bourinet V., Raguin T., Fortin M., Chetrit E., Guinde J., Laroumagne S., Fahkry N., Astoul P., Debry C., Dutau H.: Experience with transcordal silicone stents in adult laryngotracheal stenosis: a bicentric retrospective study. *Respiration* 95(6) (2018) 441-448.
- [6] Guernelli N., Bragaglia N.R.B., Briccoli A., Masrotrilli M., Vecchi R.: Tracheobronchial ruptures due to cuffed carlens tubes. *The Annals of Thoracic Surgery* 28 (1) (1979) 66-68.
- [7] Puskas J.E., Chen Y.: Biomedical application of commercial polymers and novel polyisobutylene-based thermoplastic elastomers for soft tissue replacement. *Biomacromolecules* 5(4) (2004) 1141-1154.
- [8] Sameoto D., Wasay A.: Materials selection and manufacturing of thermoplastic elastomer microfluidics. *Proceedings of the 13th Conference Microfluidics, BioMEMS and Medical Microsystems, San Francisco* (2015)
- [9] Drobny J.G.: Applications of thermoplastic elastomers. *Handbook of thermoplastic elastomers* (2015) 301-337.
- [10] Asami T., Nitta K.: Morphology and mechanical properties of polyolefinic thermoplastic elastomer I. Characterization of deformation process. *Polymer* 45(15) (2004) 5301-5306.
- [11] Shanks R., Kong I.: *Thermoplastic Elastomers, Thermoplastic Elastomers*, Prof. Adel ElSonbati (Ed.), ISBN: 978-953-51-0346-2, InTech, Available from: <http://www.intechopen.com/books/thermoplastic-elastomers/thermoplastic-elastomers>
- [12] Rzymiski W., Radusch H.: Nowe elastomery termoplastyczne. *Polimery* 4(L) (2005) 249-254.

COLLAGEN - STRUCTURE, PROPERTIES AND APPLICATION

ALEKSANDRA OWCZARZY^{1*} , ROBERT KURASIŃSKI² , KAROLINA KULIG¹ , WOJCIECH ROGÓŻ¹ , AGNIESZKA SZKUDLAREK¹ , MAŁGORZATA MACIĄZEK-JURCZYK¹ 

¹ DEPARTMENT OF PHYSICAL PHARMACY, FACULTY OF PHARMACEUTICALS SCIENCES IN SOSNOWIEC, MEDICAL UNIVERSITY OF SILESIA IN KATOWICE, UL. JAGIELLOŃSKA 4, 41-200 SOSNOWIEC, POLAND
² CARDIOLOGY CENTER, SZPITALNA 1, 41-219 SOSNOWIEC, POLAND
 *E-MAIL: AOWCZARZY@SUM.EDU.PL

Abstract

Collagen is the dominant component of the extracellular matrix of mammals. It occurs almost in all animal tissues. Collagen is a highly heterogeneous protein. The collagen protein family is characterized by great diversity in terms of structure, occurrence, and function. Up till now, 29 types of collagen proteins have been classified. The representation of individual types of collagen has certain common features. The most important property is the above-average mechanical strength that results directly from the spatial structure. Collagen is a building material for most tissues and organs. It also plays an important role in the process of cell growth and differentiation, which results from the specific structure of collagen fibers as well as their ability to adhere. The development of research techniques allowed to study in detail the molecular structure and properties of collagen. Therefore, collagen has become a subject of interest in many branches of science. Synthetic recombinant collagen fibers were developed as the basis of collagen biomaterials for medical applications, including implantology or gynecology. The specific structure of collagen also makes it applicable as a protein carrier in drug delivery systems (DDS), particularly in the treatment of cancer and genetic diseases. The use of tissue regenerative abilities and an interdisciplinary look at the properties of collagen and collagen-based biomaterials may constitute the future of medical development.

Keywords: collagen, collagen structure, physicochemical properties, biological properties, DDS, physicochemical techniques, atelocollagen

[*Engineering of Biomaterials* 156 (2020) 17-23]

doi:10.34821/eng.biomat.156.2020.17-23

Introduction

Collagen constitutes about 25% of all human proteins. Its name refers to the family of collagen proteins which differ in characteristic, location, molecular and spatial structure. Collagen is highly heterogeneous. Fibers chains are coded by different genes and biosynthesized in various tissues. Specific features of individual collagen types are the result of differences in post-translational modifications. Collagen is the dominant element of connective tissue extracellular matrix (ECM). Due to its physicochemical properties, collagen is responsible for the integrity, strength and elasticity of tissues. This natural biopolymer is constantly synthesized in the body by various cells in different amounts, depending on the current demand. Collagen plays an important role in the healing process, tissue growth, regeneration, and also participates in the processes of cells adhesion, growth and differentiation. These collagen functions take place mainly due to the specific structure of its fibers. This spatial structure, called a superhelix, provides the beneficial properties of collagen, especially very high mechanical strength [1-4].

The characteristic features of collagen fibers, their common occurrence, and relatively easy accessibility are still of interest to scientists from different research fields. In certain areas of medicine and industry collagen has been widely used as a biopolymer compatible with the human body. Yet the use of collagen as a biomaterial is still being explored [5].

Collagen structure

A basic structural unit of collagen is tropocollagen - α -helix left-handed molecule, composed of three polypeptide, spirally wound chains. Collagen fibers are formed through the aggregation of tropocollagen molecules by the electrostatic and hydrophobic side bonds. Further aggregation creates cross-links, such as covalent or non-covalent bonds between the fibrils Lysine - Lysine (Lys-Lys) and Hydroxyproline - Hydroxyproline (Hyl-Hyl) amino acids pairs [1,6,7].

The structure of the collagen molecule mainly results from the interaction between the components building polypeptides. The amino acids composition and their amount in polypeptide chains differ between different types of collagen. However, they show some common structural features. Six different types of subunits have been described and they consist of three identical (homotrimer) or three different (heterotrimer) chains or the mixture of the same two and one different chains. The collagen molecule does not only consist of helical fragments - the non-helical domains are also characteristic for some types of collagen [1,3,6].

Glycine (Gly) is the main collagen amino acid. It is about every third amino acid residue in a single polypeptide chain (approx. 35%). Proline (Pro) is the second abundant amino acid, present in an amount of 12% of all amino acids. Rarely occurring but important are lysine (Lys) and alanine (Ala), as well as aspartic (Asp), glutamic (Glu) and arginine (Arg) amino acids. A characteristic feature of the collagen molecular structure is the occurrence of nearly equimolar amounts of basic and acidic amino acids. In addition, a significant concentration of hydroxyproline (Hyp) and hydroxylysine (Hyl) can be distinguished in the composition of the polypeptide chain. These two amino acids are already formed in the post-translational and enzymatic protein processing and are responsible for the formation of higher-order structures [1,3,6,8].

Collagen-forming polypeptide chains are characterized by the presence of repeatable amino acid sequences, where the most common sequence is proline and the next one - Gly-Pro-Hyp (FIG. 1).

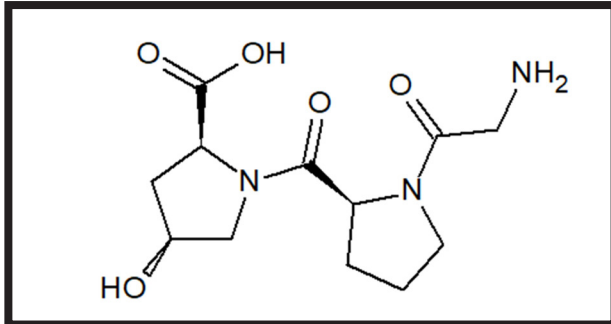


FIG. 1. The structural formula of Gly-Pro-Hyp amino acid sequence.

A slightly less common amino acid sequence is Gly-Pro-Ala. This repeatability is important for the collagen spatial structure. The systematic presence of Gly allows the formation of hydrogen bonds between its molecules. Consistency and regularity are the most important factors that significantly increase the strength of the entire helical structure. The aqueous environment plays an important role in this process as it stabilizes the hydrogen bonds. However, it has been proved that if the structure regularity is interfered the collagen molecule shows considerable flexibility. It means that the lower regularity in amino acid sequence, the greater number of kinks in the polypeptide chain. This relationship determines the elasticity of collagen molecule [3,4,6-10].

There are 29 types of collagen. The classification has been presented in FIG. 2.

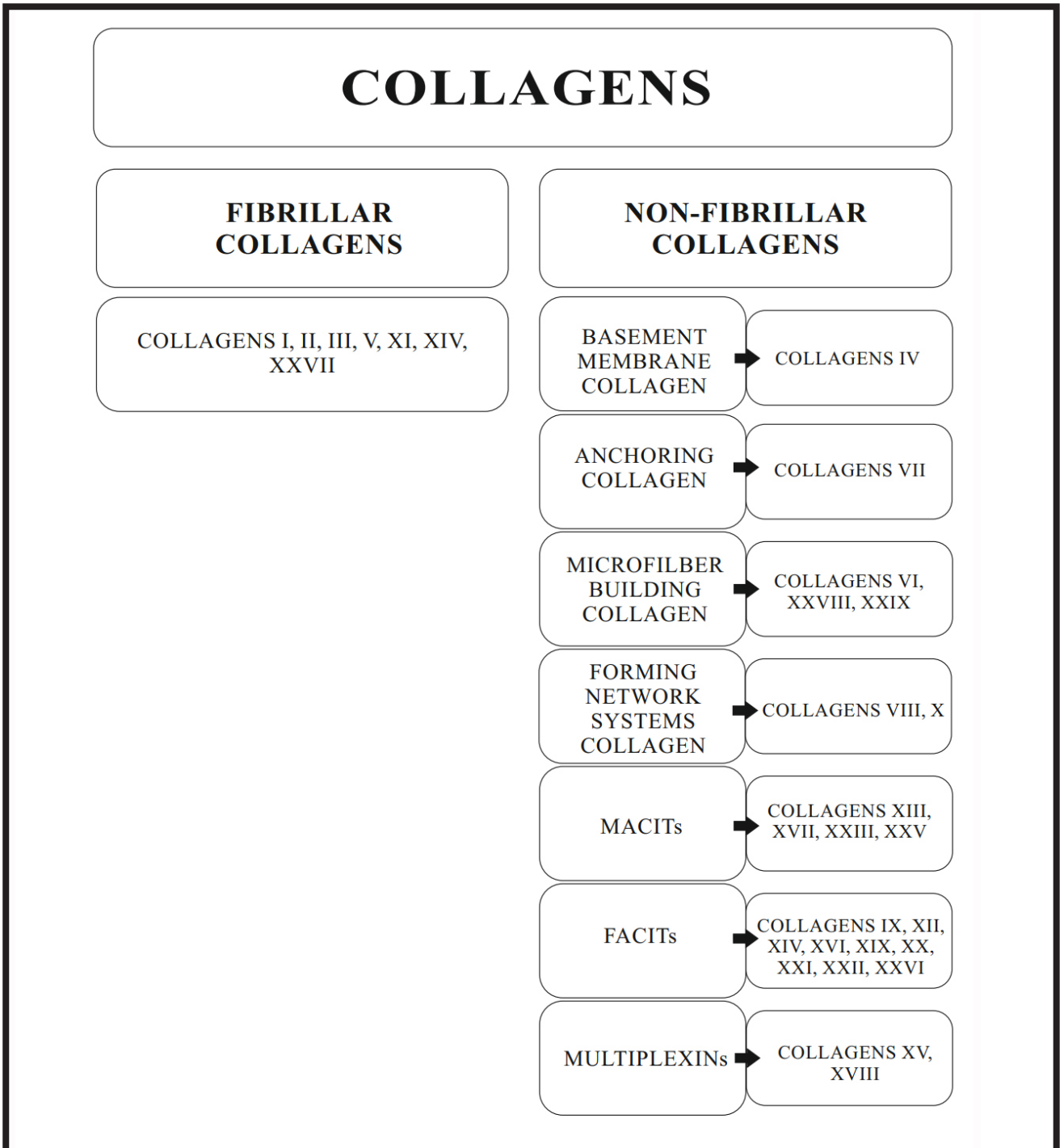


FIG. 2. The collagen proteins family.

The collagen proteins family classification is based on the differences in structure, location and properties of individual types. The two main collagen groups are: fibrillar collagen and non-fibrillar one [11,12]. Fibrillar collagen forms fibrils, constituting about 90% of all collagen presented in the human body. It is encoded by 11 genes and formed from three helically rolled up polypeptide chains, separated by short non-helical fragments called teleopeptides. The spatial structure of fibrillar collagen is cross-striated with transverse bands repeating every 64–67 nm. Non-fibrillar collagen is much more differential in terms of structure, location and properties. Although it amounts only to 10% of all the collagen in the human body, it is a vital part of many organs [8,13-15].

TABLE 1 presents the types of fibrillar and non-fibrillar collagen with examples of their location in tissues.

TABLE 1. Location of a) fibrillar and b) non-fibrillar collagen in tissues. Adapted from [12] with additional data from: [8,11,13-15].

a) Fibrillar Collagen	
Collagen Type	Location
I	skin, bones, tendons, cornea
II	gristle, vitreous body
III	skin, vessels, intestine, uterus
V	skin, bones, cornea, placenta
XI	gristle, intervertebral disc
XXIV	bones, cornea
XXVII	gristle
b) Non-fibrillar Collagen	
Collagen Type	Location
IV	basal membrane, capillaries
VI	bones, vessels, skin, cornea, gristle
VII	mucous membranes, skin, bladder, umbilical cord, amniotic fluid
VIII	skin, brain, heart, kidneys, vessels, bones, gristle
IX	cornea, vitreous body, gristle
X	gristle
XII	gristle, tendons, skin
XIII	skeletal muscles, heart, eye, skin, endothelial cells
XIV	vessels, eye, nerves, tendons, bones, skin, gristle
XV	capillary vessels, ovaries, heart, testicles, skin, placenta, kidneys
XVI	heart, skin, kidneys, smooth muscle
XVII	skin
XVIII	kidneys, lungs, liver
XIX	skin, kidneys, liver, placenta, spleen, prostate gland
XX	corneal epithelium
XXI	stomach, kidneys, vessels, heart, placenta, skeletal muscles
XXII	tissue connections
XXIII	metastatic carcinogenic cells
XXV	eye, brain, heart, testicles
XXVI	testicles, ovaries
XXVIII	nervous system cells
XXIX	skin

Collagen biosynthesis

The collagen protein family is coded by 44 genes located on the 17th pair of chromosomes. Collagen biosynthesis consists of many steps and occurs in different regions inside and outside the cell [8]. The beginning of this process does not differ much from the synthesis of every other protein in the human body. The biosynthesis begins with the transcription of genetic information in the cell nucleus, then the mRNA transcript leaves out the nucleus and goes to the endoplasmic reticulum (ER) where the genetic information is translated. As a result of this process, a new molecule, called pre – procollagen, is formed. Pre – procollagen in its structure contains a signal peptide fragment that is responsible for identifying and delivering the polypeptide molecule to the appropriate place in the ER. The other characteristic fragments of this chain are the terminal fragments located at both ends. Thanks to them proper polypeptide chains are selected to form procollagen α helix. They also prevent the premature formation of collagen fibrils [2,4].

The post-translational modification consists of three steps and takes place in the ER. First, the signal peptide is cut off, using a signal peptidase. Next, the Lys and Pro hydroxylation takes place with the participation of lysine hydroxylase, prolyl-4-hydroxylase and prolyl-3-hydroxylase. This is one of the primary stages of collagen biosynthesis that requires an appropriate environment reaction, which is provided by the presence of ascorbic acid, molecular oxygen, iron ions (II) and α -ketoglutarate. Due to the post-translational modification, it is possible to create hydrogen bonds stabilizing the spatial structure of this protein [2,4,11,16].

The final step of post-translational modification is glycosylation. The reaction occurs in the presence of glucosyltransferase and galactosyltransferase while glucose or galactose is attached to the Hyp residues. The formed polypeptide chains have an ability to self-aggregate and the new aggregated structure is called procollagen. Procollagen is stabilized by hydrogen and disulfide bonds and the oligosaccharide fragments get attached to its molecule in the Golgi apparatus. It is the last modification before the procollagen transport to the ECM [2,4]. In ECM, using N – proteinase and C – proteinase, the terminal propeptides are removed and tropocollagen is formed. Tropocollagen is able to aggregate with tropocollagen molecules spontaneously, thus forming collagen fibrils. Collagen fibrils are the final stage of collagen protein biosynthesis [2,4]. Collagen biodegradation in the body is a complicated process that can be divided into two types: extracellular and intracellular [2]. The intracellular biodegradation occurs in the process of collagen endocytosis by cells capable of phagocytosis [2,5], while extracellular biodegradation occurs due to extracellular matrix metalloproteinases (MMPs). After their activation, the triple helix spatial structure is destroyed through the degradation of peptide bonds between the pairs of amino acids: glycine-isoleucine and glycine-leucine. The collagen molecule disintegrates into two molecules in a ratio 3:1. The collagen disintegration products denature and become water-soluble in the environment [1,2,17,18].

The collagen synthesis in the human body depends on the constitutional specifics, yet it is conditioned by environmental factors. For instance, the collagen precursors synthesis (pro-collagen) can be stimulated by mechanical stress. It has been shown that collagen synthesis and degradation increase under the influence of short-term and long-term exercise [19]. Chang J. et. al. proved that the collagen synthesis may alter during 24 h cycles. Such a conclusion was based on the transmission electron microscopy observations of Achilles tendons extracted from mice [20].

Collagen in medicine – physicochemical and biological properties

The physicochemical properties of collagen are the result of its molecular structure. The most important features of collagen proteins include very high tensile and tear strength which protects the tissue against mechanical damage. The collagen fibers resistance to mechanical forces increases in direct proportion to the fiber age and cross-linking. This cross-linking is also associated with the fact that collagen binds the remaining elements of the ECM, ensuring the integrity of the tissues it occurs in. [1-3].

Due to the spatial structure of superhelix and its ability to retain water, collagen is insoluble in water. This feature makes its resistant to proteolytic enzymes, such as trypsin, chymotrypsin or pepsin. Water solubility plays a significant role in the proper biochemical process. However, this process can be limited by adding sulphate anions (IV) and (VI), metal cations Na^+ and K^+ , as well as a solution of NaCl [1,2].

Depending on the temperature, collagen denatures in two steps. This process is slower and slightly different from other proteins. In the first stage, the superhelix structure is broken by the hydrophobic and hydrogen bonds degradation and this process is reversible. In the next stage, the helical structures are destroyed and transformed into globular ones. The temperature range necessary for the collagen degradation is between 5°C and 50°C , depending on the molecule structure and the reaction conditions (pH, the concentration of salts and electrolytes and amount of hydroxyproline residues in collagen). Collagen changes its consistency, plasticity and viscosity under the thermal treatment or due to various solutions of acids and bases, both inorganic and organic. The knowledge of these properties was crucial to determine the preparation methods and obtain collagen proteins for research [13,21-23].

In addition to supporting and building functions, collagen has the ability to bind ligands of various origins, thus taking an indirect part in the biochemical processes in the surrounding tissue. Collagen binds to integrins and other mediator proteins, thereby they mediate the cells signal transmission, regulate the cells proliferation and proper migration inside the tissue. They also interact with proteoglycans, providing specific tissues with appropriate mechanical properties. Biosynthesis and biodegradation are also dependent on the collagen binding to other substances, such as collagenases or protein chaperones [24,25].

Collagen is also involved in the process of neoplastic cell formation, angiogenesis and metastasis. The tumor micro-environment influences the ECM, resulting in the deposition of fibronectin, proteoglycans and collagen types I, III, IV. It promotes tumor progression through the increased mutual cells adhesion, cells polarity disorders, and the increasing growth factor signaling [26].

Moreover, collagen has a positive effect on the proper immune system functioning, mainly through the impact on the complement system functioning. Collagen also binds the C1r or C1s components that are responsible for activating the system and enhancing the immune response. Due to the characteristic spatial structure, collagen also has the ability to nonspecific binding of polyanionic compounds, such as oxidized low-density lipoprotein (LDL). The list of ligands that can be bound by collagen is very long and is constantly expanding. Some of them bind only to a specific type of collagen, while others bind nonspecifically and more spontaneously. Unfortunately, not all ligand binding regions in the collagen molecule have been accurately characterized and described [27-34].

Thanks to the detailed knowledge of the molecular structure and physicochemical properties, collagen has become an object of interest in many scientific areas, e.g. nanotechnology or biomedical engineering. Numerous studies have allowed to create synthetic, recombinant collagen fibers to produce collagen biomaterials with different structure and function [12,35,36].

Among others, collagen-based biomaterials engage atecollagen. It is the type I collagen derivative deprived of telopeptide fragments that are responsible for the lack of immunogenicity. Due to low toxicity, antigenicity, common occurrence and ease of obtaining, collagen is a safe building unit for materials synthesis. Collagen-based materials are biocompatible and biodegradable. They are often used in reconstructive medicine, implantology and pharmacology [12,35,37].

Insoluble and porous collagen sponges are one of the many collagen-based biomaterials. They are formed during the lyophilization of acid or alkaline animal collagen aqueous solutions. The sponges pore size can be controlled during production and depends on the amount of dry collagen mass and the speed of solution freezing. Collagen sponges are able to absorb liquids. During the production process, they are enriched by elastin, glycosaminoglycans or fibronectin, making them more flexible. Additional cross-linking of these materials, using glutaraldehyde and conjugated with poli(hydroxyethylmethacrylate), increases their mechanical strength.

Collagen sponges are used in medicine as a dressing for burn wounds and bedsores. They can be soaked with antibiotics, usually gentamicin, acting as drug carriers. Collagen sponges protect tissue against infection. The presence of opened and semi-closed pores in collagen sponges allows for the quick and prolonged local effect of the drug, which depends on the biodegradation rate. The advantage of this type of biomaterials is also a possibility to obtain the maximum drug concentration in the appropriate place and to reduce the side effects during the antibiotic therapy [12,18,35,36,38].

In the structure of collagen hydrogels, there are numerous dispersed water molecules. They can be formed in the process of spontaneous polymerization which already takes place in physiological conditions. The spatial structure of collagen gels is maintained thanks to strong electrostatic interactions and hydrophobic bonds. Due to the large fluid accumulation inside the gel, they have the ability to effectively exchange ions and metabolites with the surrounding tissue. The rich cross-linking of collagen gels is the reason for keeping fluids inside the biomaterial structure, which affects its characteristic mechanical properties and application. Collagen hydrogels can be compressed, in a more or less controlled manner, depending on the application.

Due to their properties and structure similar to soft tissues, collagen gels have found wide clinical application. Microgels based on collagen type I are mainly used. Depending on the type of cells, they can be used to regenerate and rebuild different types of tissues. Collagen type II is also used in hydrogels. Its structure and functionality resembles cartilage. It stimulates the differentiation of mesenchymal stem cells towards chondrocytes, therefore collagen type II gels have been used in the regeneration of this type of tissue. The examples of hydrogel applications are presented in TABLE 2 [12,35,36,38].

TABLE 2. Hydrogels in medicine. Adapted from: [12,18,35,36,38].

Types of collagen	Types of cells	Application
Collagen type I	Fibroblasts	Dermis regeneration
	Cardiomyocytes	Heart muscle reconstruction
	Growth factors and polypeptides	Promote polarity nerve cells, alignment and increase adhesion
Collagen type II		Cartilage regeneration

TABLE 3. Examples of the use of collagen as a biomaterial in medicine. Adopted from [12,18].

Medicine area	Biomaterial form	Application
Skin regeneration	Collagen type I hydrogels with fibroblasts	Reproduction of skin defects
	Compensated collagen hydrogels	Skin reconstruction <i>in vitro</i> and <i>in vivo</i>
	Hydrogel with liposomes	Drug delivery in skin during regeneration, accelerating the wound healing process
	Collagen sponges	Treatment of severe burns and bedsores
Dental surgery and implantology	Collagen membranes	Post-implant skin regeneration, closure of sinus fistulas, treatment of bone and cartilage tissue defects
Ophthalmology	Collagen films and membranes	Treatment of corneal defective, reconstruction of the corneal epithelium after surgical removal, drug delivery to the surface of the eyeball
Urology/Gynecology	Collagen materials containing bladder cells, muscle cells or fibroblasts	Bladder plastic surgery, treatment of urethral stricture
Orthopedics	Scaffold based on polyurethane with collagen type I hydrogel and TGF β -1 [45], sponge structure collagen implants [46]	Treatment of vertebrae [45]. collagen meniscus (Menaflex - CMI, ReGen Biologics, Franklin Lakes, New Jersey) [46]
Laryngology	Collagen hydrogel, autologous grafts from skin [47]	Nestorian function of vocal cords and epiglottis [47]
Neurology (in the experimental stages)	Various collagen materials	Peripheral nerves regeneration
Aesthetic medicine	Masks, gels, creams, injection preparations	Wrinkle filling, scar regeneration, improve facial contours, lips, overall skin improvement

Collagen films are very thin and durable. The film thickness is between 0.1 to 0.5 mm. They are formed by evaporating the solution that may contain medical substances, such as gentamycin or tetracyclines. Collagen films and membranes are useful in ophthalmology, in the treatment of corneal infections and wound healing. They can also be used indirectly to cover other biomaterials to change their surface properties. Collagen films containing rapamycin are used in the production of coronary stents and drug-free collagen film are used to produce lenses. Their function is protecting lenses from mechanical damage [12,35,36,38]. The examples of using biomaterial are presented in TABLE 3.

Collagen can be also used as a protein carrier in drug delivery systems (DDS). Their function is to deliver an old and new generation drug to the destination inside the body [39]. The connection between the carrier and the drug substance occurs thanks to the formation of a covalent bond. The carrier may be atelocollagen. This completely safe biomaterial has a positive charge to facilitate the transfer of pharmaceuticals. Collagen protein in drug delivery systems is primarily used to transport proteins and nucleic acids. It is applicable to treat cancer and genetic diseases. TABLE 4 presents the examples of drugs transported using DDS [34,39,40].

TABLE 4. Examples of drugs transported using DDS. Adapted from: [35,37-39].

Drug	Application
Interferon	Viral diseases treatment
Interleukin - 2	Immune deficiencies
Nerve Growth factor (NGF)	Central nervous system diseases treatment
Basic Fibroblast Growth Factor (bFGF)	Fracture treatment

Physicochemical techniques of collagen analysis

The complexed spatial structure and physicochemical properties of collagen can be analyzed using various techniques. The constantly expanding knowledge on this subject makes it possible to apply different collagen types as building materials in the medical industry [32,33,41].

To assess the structure of collagen fibers, two complementary techniques: transmission electron microscopy (TEM) and synchrotron X-ray scattering can be used. TEM provides information about local structural on the scale of 15 nm to several micrometers, while X-ray scattering gives general information about the packing collagen molecules. The morphology of fibrils and of whole collagen membranes can also be observed using a scanning electron microscope (SEM), however, this technique requires specific chemical preparation of the tested material [32,33,35]. TEM enables the analysis of collagen in biological systems, X-ray scattering can be used to investigate the structural features of fibrillar human collagen, while SEM – collagen morphology.

To determine the thermal stability of collagen and its derivatives, differential scanning calorimetry (DSC) is used. Miles et al. used DSC to determine the thermal stability of native and artificially cross-linked collagen, derived from rat tail tendon at different levels of hydration [42]. DSC can be used for thermal analysis during the collagen treatment and inflammatory pathological states (besides the classical histological methods).

The structural properties of collagen proteins can be described by circular dichroism (CD). CD describes the secondary structure and it determines the triple helix – the presence, profile and stability. This technique can also be used to assess the optical ability of collagen solutions and to monitor conformation changes in the structure of the polymer triple helix. CD in the wavelength range from 100 to 200 nm (vacuum ultraviolet - VUV) can also be used to determine the purity of collagen samples [43,44]. Spectroscopy CD could be helpful in the analysis of collagen based on biomaterials exposed to chemical and physical agents during their manufacturing for medical purposes.

In order to assess the collagen fibers elasticity, nuclear magnetic resonance spectroscopy (NMR) can be used [8]. NMR spectroscopy can also assess collagen in native ECM. The way collagen molecules move provides information about its mechanical and biological properties. Another interesting method to assess the collagen molecular structure without damage is the solid state NMR spectroscopy, performed both in vivo and in vitro. This technique can provide information about the aging process of collagen fibers and/or their molecular changes under the influence of an ongoing disease [47].

Summary

The collagen protein family is characterized by mechanical strength resulting from the spatial structure, wide structure diversity, occurrence and function. The super helical structure is unique in the world of animal proteins.

The regenerative potential of the human body is still the subject of numerous studies. Taking advantage of natural tissue regenerative abilities, along with the application of new technologies and biomaterials, is the future of medicine. The knowledge about collagen has gradually expanded with the progress of research techniques, enabling a thorough investigation of their structure. These proteins still remain a subject of research and our knowledge is not complete. Characteristic features, such as strength and common occurrence, have facilitated the use of collagen as a biomaterial for many clinical purposes. An interdisciplinary look at the possibilities of using collagen and biomaterials created on its basis can help to develop medicine and other scientific areas.

Statement

This paper received no specific grant from any funding agency in the public, commercial, or non-profit sectors.

ORCID iDs

A. Owczarzy:	 https://orcid.org/0000-0003-1571-9643
R. Kurasiński:	 https://orcid.org/0000-0002-2789-5006
K. Kulig:	 https://orcid.org/0000-0001-9198-2254
W. Rogóż:	 https://orcid.org/0000-0002-6649-3480
A. Szkudlarek:	 https://orcid.org/0000-0002-6891-9625
M. Maciążek-Jurczyk:	 https://orcid.org/0000-0003-1054-6309

References

- [1] Meyer M.: Processing of collagen based biomaterials and the resulting materials properties. *BioMedical Engineering OnLine* (2019)
- [2] Morağ M., Burza A.: Budowa, właściwości i funkcje kolagenu oraz elastyny w skórze. *Journal of Health Study and Medicine* 2 (2017) 77-100.
- [3] Birk D.E., Bruckner P.: *Collagen Suprastructures*. Collagen. Springer (2015) 185-205.
- [4] Brodsky B., Ramshaw J.: The collagen Triple – Helix Structure. *Matrix Biology* (1997) 545-554.
- [5] Wagenaar-Miller R., Engelholm L., Gavard J., et al.: Complementary Roles of Intracellular and Pericellular, Collagen Degradation Pathways In Vivo. *Molecular and Cellular Biology* (2007) 6309-6322.
- [6] Burjanadze T.V.: New analysis of the Phylogenetic Change of Collagen Thermostability. *Biopolymers* 53 (2000) 523-528.
- [7] Domene C., Jorgensen C., Wajid Abbasi S.: A perspective on structural and computational work on collagen. *Physical Chemistry Chemical Physics* 18 (2016) 24802-24811.
- [8] Czubak K., Żbikowska H.: Struktura, funkcja i znaczenie biomedyczne kolagenów. *Annales Academiae Medicae Silesiensis* 68 (2014) 245-254.
- [9] Shoulders M., Raines R.: Collagen Structure and Stability. *Annual Review of Biochemistry* 78 (2009) 929-958.
- [10] Brodsky B., Persikov A.: Molecular structure of the collagen triple helix. *Advanced in Protein Chemistry* 70 (2005) 301-339.
- [11] Ricard-Blum S.: The Collagen Family. *Cold Spring Harbor Perspectives in Biology* (2011) 1-19.
- [12] Sorushanova A., Delgado L., Wu Z., et al.: The Collagen Suprafamily: From Biosynthesis to Advanced Biomaterial Development. *Advanced Materials* 31 (2019) 1801651.
- [13] Gelse K., Pöschl E., Aigner T.: Collagens – structure, function, and biosynthesis. *Advanced Drug Delivery Reviews* 55 (2003) 1531-1546.
- [14] Holmes D., Lu Y., Starborg T., et al.: Collagen Fibril Assembly and Function. *Current Topics in Developmental Biology* 130 (2018) 107-142.
- [15] Mienaltowski M.J., Birk D.E.: Structure, physiology, and biochemistry of collagens. *Advances in Experimental Medicine and Biology* 802 (2014) 5-29.
- [16] Granner D.K.: Synteza białek i kod genetyczny. *Biochemia Harpera*, Murray RK, Granner DK, Mayes PA, Rodwell V. W. Wydawnictwo Lekarskie PZWL (1995) 491-507.
- [17] Sprangers S., Everts V.: Molecular pathways of cell-mediated degradation of fibrillar collagen. *Matrix Biology* 2017.
- [18] McKleroy W., Lee T.H., Atabai K.: Always cleave up your mess: targeting collagen degradation to treat tissue fibrosis. *American Journal Of Physiology Lung Cellular and Molecular Physiology*. 304 (2013) 709-721.
- [19] Strzyż P.: Collagen around the clock. *Nature Review Molecular Cell Biology* (2020)
- [20] Gauza M., Kubisz L., Przybyłski J.: Właściwości preparatów kolagenowych ze skór ryb pozyskiwanych metodą kwaśnej hydratacji. *Nowiny Lekarskie* 79 (2010) 157-162.
- [21] Engel J.: Investigation of the Denaturation and Renaturation of Soluble Collagen by Light Scattering. *Archives of Biochemistry and Biophysics* 97 (1962) 150-158.
- [22] Harkness R.: Biological functions of collagen. *Biological review* 36 (1961) 399-463.
- [23] Wahyudi H., Reynolds A.A., Li Y., et al.: Targeting collagen for diagnostic imaging and therapeutic delivery. *Journal of Controlled Release* 240 (2016) 323-331.
- [24] Jikko A., Harris S.E., Chen D., et al.: Collagen Integrin Receptors Regulate Early Osteoblast Differentiation Induced by BMP-2. *Journal of Bone and Mineral Research* 14 (1999) 1075-1083.
- [25] Fang M., Yuan J., Peng Ch., Li Y.: Collagen as a double-edged sword in tumour progression. *Tumour Biology* 35 (2014) 2871-2882.
- [26] Jokinen J., Dado E., Nykivist P., et al.: Integrin – mediated Cell Adhesion to Type I Collagen Fibrils. *The Journal of Biological Chemistry* 279 (2004) 31956-31963.
- [27] Ruggeri A., Benazzo F.: Collagen – proteoglycan interaction. Ultrastructure of the Connective Tissue Matrix. *Electron Microscopy in Biology and Medicine book series* (1984) 113-125.
- [28] Broom N., Silyn-Roberts H.: Collagen – Collagen Versus Collagen Proteoglycan Interactions in the Determination of Cartilage Strength. *Arthritis & Rheumatology* 33 (1990) 1512-1517.
- [29] Burkhardt H., Sehnert B., Bockermann R., et al.: Humoral immune response to citrullinated collagen type II determinants in early rheumatoid arthritis. *European Journal of Immunology* 35 (2005) 1643-1652.
- [30] Krieger M., Herz J.: Structures and Functions of multiligand lipoprotein receptors and LDL Receptor – Related Protein (LRP). *Annual Review of Biochemistry* 63 (1994) 601-637.
- [31] Gobeaux F., Mosser G., Anglo A., et al.: Fibrillogenesis in dense collagen solutions: a physicochemical study. *Journal of Molecular Biology* 376 (2008) 1509-1522.
- [32] Besseau L., Giraud-Guille M. M.: Stabilization of fluid cholesteric phases of collagen to ordered gelled matrices. *Journal of Molecular Biology* 251 (1995) 197-202.
- [33] An B., Lin Y., Brodsky B.: Collagen interactions: Drug design and delivery. *Advanced Drug Delivery Reviews*. 97 (2016) 69-84.
- [34] Chattopadhyay S., Raines R.: Collagen – Based Biomaterials for Wound Healing. *Biopolymers* 101 (2014) 821-833.
- [35] Turek A., Kasperczyk J., Dzierżewicz Z.: Zastosowanie kolagenu w technologii postaci leku. Osiągnięcia i perspektywy. *Chemik* 64 (2010) 1-5.
- [36] Lynn A.K., Yannas I.V., Bonfield W.: Antigenicity and immunogenicity of collagen. *Journal of Biomedical Materials Research* 71 (2004) 343-354.
- [37] Lee C.H., Singla A., Lee Y.: Biomedical applications of collagen. *International Journal of Pharmaceutics* 221 (2001) 1-22.
- [38] Wysocki T., Sacewicz I., Wiktorska M., et al.: Atelokolagen jako potencjalny nośnik terapeutycznych. *Postępy Higieny i Medycyny Doświadczalnej* 61 (2007) 646-654.
- [39] Nevozhay D., Kańska U., Budzyńska R., et al.: Współczesny stan badań nad koniugatami i innymi systemami dostarczania leków w leczeniu schorzeń nowotworowych i innych jednostek chorobowych. *Postępy Higieny i Medycyny Doświadczalnej* 61 (2007) 350-360.
- [40] Zhang Z., Guoying L., Shi B.: Physicochemical Properties of Collagen, Gelatin and Collagen Hydrolysate Derived from Bovine Lined Split Wastes. *Journal of the Society of Leather Technologists and Chemists* 90 (2006) 23-28.
- [41] Miles C., Avery N., Rodin V., et al.: The increase in denaturation temperature following cross – linking of collagen is caused by dehydration of the fibres. *Journal of Molecular Biology* 346 (2005) 551-556.
- [42] Jenness D., Sprecher C., Johnson Jr W.: Circular Dichroism of Collagen, Gelatin, and Poly(proline) II on in the Vacuum Ultraviolet. *Biopolymers* 15 (1976) 513-521.
- [43] Bhatnagar R.S., Gough C.A.: Circular Dichroism of Collagen and Related Polypeptides: Circular Dichroism and the Conformational Analysis of Biomolecules. *Protein Science* (1996) 183-199.
- [44] Du J., Long R.G., Nakai T., et al.: Functional cell phenotype induction with TGF-β1 and collagen-polyurethane scaffold for annulus fibrosus rupture repair. *European Cell & Material* 39 (2020) 1-17.
- [45] Harston A., Nyland J., Brand E., et al.: Collagen meniscus implantation: a systematic review including rehabilitation and return to sports activity. *Knee Surgery, Sports Traumatology, Arthroscopy* 20 (2012) 135-146.
- [46] Tang S.S., Mohad V., Gowda M., Thibeault S.L.: Insights Into the Role of Collagen in Vocal Fold Health and Disease. *Journal of Voice* 31 (2017) 520-527.
- [47] Goldberga I., Li R., Duer M.J.: Collagen Structure–Function Relationships from Solid-State NMR Spectroscopy. *Accounts of Chemical Research* 51 (2018) 1621-1629.

THE INFLUENCE OF PROSTHETIC ELEMENTS MANUFACTURING TECHNOLOGY ON PROPERTIES AND MICROSTRUCTURE SHAPING Co-Cr-Mo ALLOYS

JOANNA AUGUSTYN-NADZIEJA^{1*} ,
AGNIESZKA SZCZOTOK² 

¹ AGH UNIVERSITY OF SCIENCE AND TECHNOLOGY,
FACULTY OF METALS ENGINEERING AND INDUSTRIAL
COMPUTER SCIENCE, DEPARTMENT OF PHYSICAL
AND POWDER METALLURGY,
MICKIEWICZA AV. 30, 30-059 KRAKOW, POLAND

² SILESIAN UNIVERSITY OF TECHNOLOGY,
FACULTY OF MATERIALS ENGINEERING,
DEPARTMENT OF ADVANCED MATERIALS
AND TECHNOLOGIES,
KRASINSKIEGO STR. 8, 40-019 KATOWICE, POLAND

*E-MAIL: JAP@AGH.EDU.PL

Abstract

The presented publication discusses the test results regarding samples of a prosthetic alloy from the Co-Cr-Mo system. The test samples were obtained by means of two different methods applied in prosthetics laboratories to compare their properties and microstructure. To obtain the samples via the traditional lost wax casting method, the cast alloy Co-Cr-Mo was used, commercially known as Wironit LA. In the case of the modern technique DMLS (Direct Metal Laser Sintering), metallic powder Co-Cr-Mo, called EOS Cobalt Chrome MP1, was used. The samples of both Co-Cr-Mo alloys obtained via the two methods were prepared for metallographic tests; they also underwent microstructural observations with the use of light microscopy (LM) and scanning electron microscopy (SEM), and next they were subjected to hardness tests. The obtained samples demonstrated a dendritic structure. In the samples cast with the lost wax casting method, a segregation of the chemical composition was revealed. The samples obtained by means of the DLMS method were characterized by chemical composition homogeneity. The hardness measurements with the statistical analysis of the measurement results showed a difference between the examined alloys. On the basis of the performed studies, it was stated that the applied methods of manufacturing prosthetic elements make it possible to obtain diversified microstructural and mechanical properties of the alloys. The hardness value significantly affects the subsequent mechanical and finishing treatment of prosthetic elements, such as metal bases of crown caps, bridges, mobile prostheses or other retention elements.

Keywords: Co-Cr-Mo alloys, dental prosthetics, lost wax casting method, selective laser sintering of metal powders (DLMS), microstructure, hardness

[*Engineering of Biomaterials* 156 (2020) 24-31]

doi:10.34821/eng.biomat.156.2020.24-31

Introduction

The modern techniques applied to recreate tooth losses have to meet growing requirements. The development of dental prosthetics provides more and more possibilities to select the optimal method of filling losses in the patient's tooth [1-3]. A group of metallic materials commonly applied in prosthetics are Co-Cr alloys with Mo and/or W microadditions [4-7]. The technology of producing metal prosthetic elements determines their microstructure [6,8-11,32], thus affecting their mechanical properties [12], corrosion resistance [13] and tribological wear [14,15,27].

One of the most popular methods used to manufacture prosthetic elements is the lost wax casting [16-18] which makes it possible to match the element with the patient's anatomy. Another frequently applied method is direct metal laser sintering (DMLS) [16,17,19]. Thanks to these methods elements of complicated shapes can be manufactured, hence the high interest in their possibilities in dental prosthetics.

The production of a metal prosthetic element via the precision casting method (lost wax technique) takes place during the casting process. In this process, a previously prepared ceramic mould based on a wax model is filled with a liquid metal alloy. The quality of the obtained casts depends largely on the metal's melting point among other factors [20,21]. Already at the beginning of the modelling process, special attention should be paid to a uniform thickness of the prosthetic element's wall [23]. In the lost wax casting method, in its first stage, a wax model representing the shape of the final prosthetic element is produced. The wax moulds are placed in a casting ring and covered with a protective body, consisting of a binding agent, such as calcium sulphate hemihydrate ($\text{CaSO}_4 \cdot 2\text{H}_2\text{O}$) and a refractory ceramic mass of quartz or cristobalite. The casting ring is left for about 45 min until the ceramic mass completely binds. The process of wax burning consists in heating the casting ring in order to harden the refractory mass and removing the wax by melting and burning. If during the ceramic mass cooling, a thermal expansion occurs, the wax burning temperature is within the scope of 500-600°C. In turn, if a hygroscopic expansion takes place during the ceramic mass cooling process, the wax burning temperature should be maintained at about 460°C [20,23]. Directly after the wax burning process, the casting process should begin so that the casting ring does not cool down significantly [23]. The liquid alloy (Co-Cr-Mo) from the temperature of 1350-1400°C is cast into a hot mould with a temperature of 800-1000°C. In order to uniformly distribute the metal in the casting mould, a centrifuge with a centrifugal force is used. In this method, the metal is introduced from the crucible where it has been melted, directly through the casting channels, into the casting mould located in the ring. The whole process in the centrifuge does not last longer than 1 second. After the casting process, the centrifuge should continue to exert pressure on the solidifying metal, as this guarantees the proper shaping of the cast edges, and the mould has to cool down. During that time, the alloy crystallization takes place. Next, the ceramic mould is broken, and the metal prosthetic element is cleaned, milled and polished [20].

It should be emphasized that producing a high-quality cast is possible only if the recommendations are met and the appropriate melting and casting temperatures for a given alloy are applied. If the parameters are improper, the cast metal element will have an inhomogeneous structure and lowered mechanical properties. Additionally, casting defects, such as pores and micro shrinkages, will occur.

In consequence, the lost wax casting makes it impossible to produce a precision cast with efficient microstructural and mechanical properties. That is why an increasing role in prosthetics laboratories is played by DMLS (Direct Metal Laser Sintering) techniques which belong to the most popular additive technologies (additive manufacturing) [24]. The laser does not sinter but completely melts the powdered material. Therefore, the obtained elements are very strong and suitable for the subsequent treatment and their structure is not weakened [25]. The dimensional accuracy grade of the DMLS techniques according to DIN EN ISO 2768 is category C, depending on the size of the detail (in practice from ± 0.15 for details of up to 100 mm to ± 0.3 for larger details, depending on the geometry type and the arrangement in the working chamber). In the series production of one detail, the process can be optimized and it is possible to obtain accuracies of more than ± 0.1 mm. The minimal wall thickness of metal prints equals 0.6 mm [26]. In the additive techniques, numerically controlled devices apply the CAD/CAM (Computer-Aided Design/Computer-Aided Manufacturing) technology. CAD systems are used to design the shape of crowns and bridges, whereas CAM makes it possible to generate a machine code based on the created CAD models.

CAM packets also visualize and simulate the production process so as to limit errors. The virtually designed components are free of imperfections that might occur in the lost wax method [20,21,27,28].

The aim of the performed research was to evaluate the effect of the two production methods, i.e. the lost wax casting method to produce a prosthetic alloy Co-Cr-Mo and the direct metal laser sintering method (DMLS) to produce metallic powder Co-Cr-Mo, on the obtained material microstructure and hardness.

Materials and Methods

The materials assigned for the tests were the Co-Cr-Mo alloys samples used to produce prosthetic elements, such as crowns, bridges, attachments and frameworks of partial dentures. Some of the test samples were obtained through remelting of the commercial alloy Wironit LA by Bego Company [29] during the lost wax casting process. The chemical composition and the mechanical properties of the alloy Co-Cr-Mo Wironit LA are presented in TABLES 1 and 2.

TABLE 1. Chemical composition of the tested Co-Cr-Mo alloy (Wironit LA), % wt. [29].

Cr	Mo	Si	C	Co
29.0	5.5	1.2	max. 0.25	rest

TABLE 2. Physical and mechanical properties of Co-Cr-Mo alloy (Wironit LA) [29].

ρ [g/cm ³]	Melting temp. [°C]	Casting temp. [°C]	E [GPa]	R _{p0.2} [MPa]	R _m [MPa]	A ₅ [%]
8.2	1300- 1340	1450	220	640	940	8

In the lost wax method, soft modelling wax was used to make models of elements measuring 3x19x19 mm which casting pins were fixed to. The construction was fixed to the base of the casting ring with a pin. The prepared protective mass was poured into the casting ring and left for 20 min until a complete solidification of the mould took place. In the following step, the ceramic mould was placed in the furnace heated up to 970°C in order to melt the wax. Next, the hot ceramic mould and the crucible with the Co-Cr-Mo (Wironit LA alloy) were placed in the centrifuge equipped with an inductive heater. The centrifuge was activated and the Co-Cr-Mo liquid alloy was pressed into the ceramic mould due to the centrifugal force. The temperature of the liquid alloy was about 1400°C. After the casting process, the mould was removed and cooled in the air until the complete alloy crystallization. At the last stage, the cast Co-Cr-Mo alloy samples were cleaned of the remains of the ceramic mass with a sandblasting unit and an abrasive disk. Next, the channels and the casting cone were cut off. A total of 10 Co-Cr-Mo samples measuring 3x19x19 mm were cast and subjected to tests.

The second batch of the test materials were the Co-Cr-Mo samples obtained via the direct laser metal sintering technique (DLMS). The EOS CobaltChrome MP1 powder was used to prepare the samples. It fulfils the chemical and mechanical specifications of the standards ISO 5832-4 and ASTM F75 for casting alloys Co-Cr-Mo assigned for implants, as well as the specifications of the standards ISO 5832-12 and ASTM F1537 for alloys Co-Cr-Mo assigned for forged elements. The chemical composition and the mechanical properties of the powder EOS CobaltChrome MP1 are presented in TABLES 3 and 4 [30].

The laser sintering process was performed with a 3D EOSINT M280 printer by means of the DMLS technique. The initial value of the laser beam equalled 1 mW, and the laser wavelength was 600-700 nm. Nitrogen was applied as a protective gas. The detail made on the printer was shaped as a cylinder measuring 140 mm in length and 10 mm in diameter. The shape and size of the produced element required the use of a support mesh to protect the element from bending during the printing, as the powder layer beneath the element did not withstand the pressure. The experiments were performed on a total of 10 Co-Cr-Mo samples measuring 10 mm in length and 10 mm in diameter.

TABLE 3. Chemical composition of the tested Co-Cr-Mo powder (EOS CobaltChrome MP1), % wt. [30].

Cr	Mo	Si	C	Mn	Fe	Co
26-30	5-7	≤ 1.0	≤ 0.16	≤ 1.0	≤ 0.75	rest

TABLE 4. Physical and mechanical properties of Co-Cr-Mo powder (EOS CobaltChrome MP1) [30].

ρ [g/cm ³]	R _{p0.2} [MPa]	R _m [MPa]	A ₅ [%]
8.3	600	1100	20

The metallographic tests of the examined Co-Cr-Mo alloys included the samples grinding and polishing in order to obtain a flat surface and their etching to reveal the microstructure. Abrasive papers (SiC) with the granularity 320, 500, 800, 1000, 1200 and 2000 μm were used for grinding and polishing cloth with an agent of a diamond suspension 3 and 1 μm was applied for polishing. The finishing treatment was conducted on a polishing cloth type OPS with the use of a diamond suspension 1/4 μm . In order to reveal the microstructure of the examined samples, the microsections were subjected to electrolytic etching. The etching reagent was a mixture of 60 cm^3 HCl, 15 cm^3 HNO_3 , 15 cm^3 CH_3COOH and 15 cm^3 distilled water and the voltage used for the electrolytic process was 4-5 V. The microstructure observations were performed with a light microscope (LEICA DM4000 M) and a scanning electron microscope (HITACHI S-3500N) equipped with an X-ray spectrometer EDS by NORAN 986B-1SPS.

The samples' hardness was measured by means of the Vickers method using a hardness tester ZWICK/ZHU 187.5, with a load of 100 N (HV10) and a measurement time of 10 s. The tests were conducted on all the 20 samples obtained by both production techniques and the number of measurements in randomly selected areas was 10. The obtained measurement results were subjected to statistical analysis. The following parameters were determined: the hardness measurement mean value ($\overline{\text{HV10}}$), the standard deviation ($s_{(\overline{\text{HV10}})}$), the absolute limiting error (δ_g) and the relative limiting error (γ_g), where $t\alpha = 1.98$ - the value read from the t-Student distribution table, dependent on the number of performed measurements, the significance level $\alpha = 0.05$ and the number of degrees of freedom $k = 9$ ($k = n - 1$, where n constitutes the number of measurements performed on the sample).

Results and Discussion

The etched Co-Cr-Mo alloys samples underwent observations by means of light microscopy. The selected micro-images of the examined alloys, both after casting by the lost wax method and after laser sintering by DLMS, are presented in FIGs 1 and 2.

The Co-Cr-Mo (Wironit LA) alloy samples (FIG. 1a-d) are characterized by the dendritic microstructure, typical of casting alloys. It is visible especially under low magnification (FIG. 1a). Based on the literature data [31], we know that the alloy's primary structure obtained directly after crystallization consists of large matrix grains constituted by a solution of chromium and molybdenum in cobalt. As a result of the structural and thermal stresses present in the material, microcracks occurred, causing a drop in the material's strength. The crack propagation proceeded in the interdendritic spaces (FIG. 3a,b).

FIG. 4a shows the typical microstructure of the cast Co-Cr-Mo alloy obtained by lost-wax casting with visible precipitates enriched in Mo and Cr. It is known that cast materials are characterized by the chemical composition micro-segregation and inhomogeneity. That is why, the SEM observations and EDS chemical composition analyses were carried out in micro-areas (FIG. 4b,c).

The chemical composition analyses performed in micro-areas of the lost-wax cast Co-Cr-Mo alloy confirmed that its matrix was constituted by a solid solution of chromium and molybdenum in cobalt (FIG. 4c). The SEM observations and the analysis of X-ray spectra revealed the phenomenon of inverse Cr micro-segregation (FIG. 3 and 4) which diffused both into the dendritic cores and the interdendritic spaces.

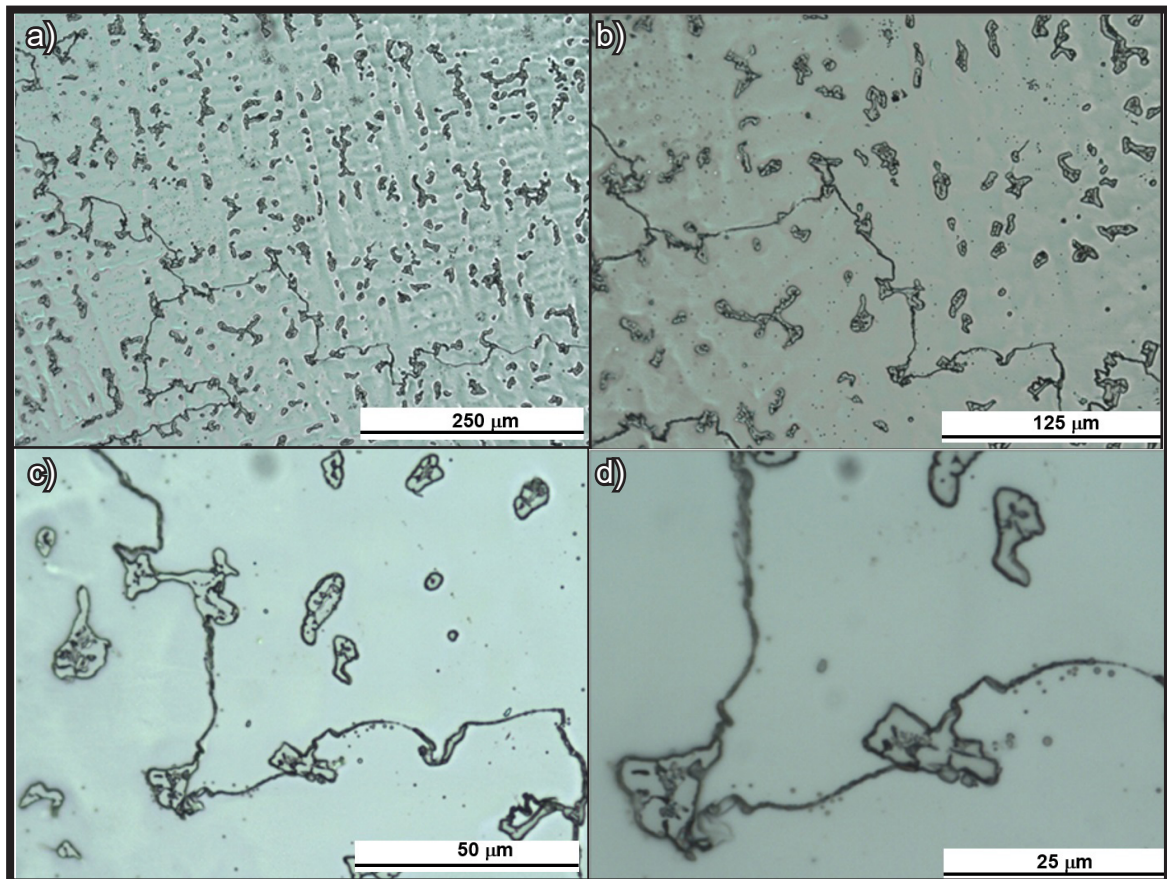


FIG. 1. Microstructure of Co-Cr-Mo alloy after the lost-wax casting method (a-d); LM, etched state.

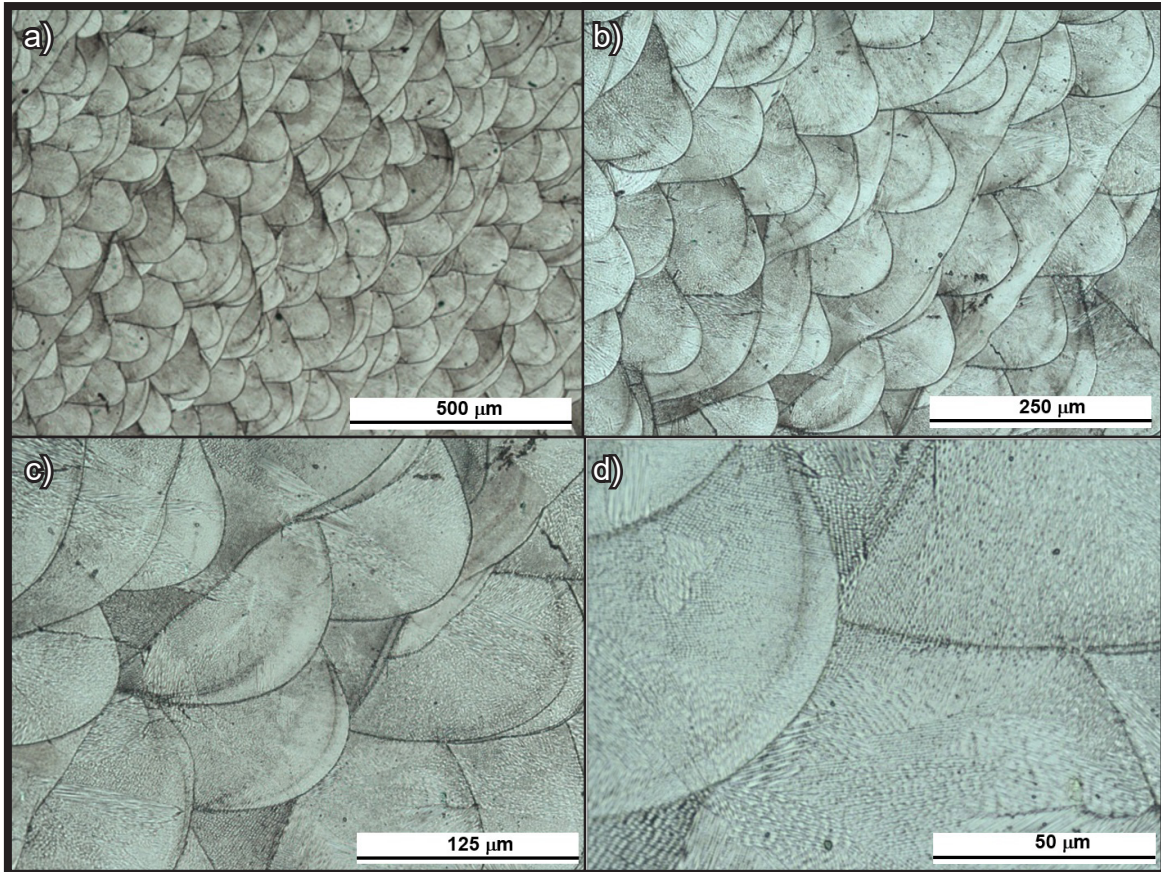


FIG. 2. Microstructure of Co-Cr-Mo alloy after selective laser sintering using the DLMS technique (a-d); LM, etched state.

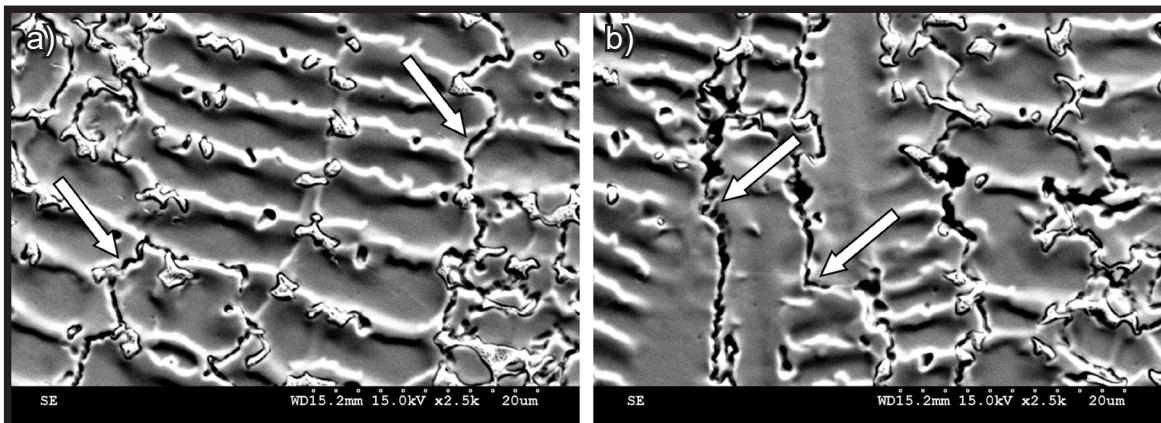


FIG. 3. Microstructure of Co-Cr-Mo alloy obtained by the lost-wax casting method with revealed microcracks in the dendritic microstructure; the images taken for different places on the sample (a, b); SEM, etched state. The arrows show examples of microcracks in the alloy.

The carbide phases are the main source of the alloy's reinforcement [10,32-34]. It is possible to notice the areas (FIG. 3a,b) between the arms of the dendrites, the so-called interdendritic spaces, where carbide phases precipitate. According to the literature data [9,18,32], type M_7C_3 and M_6C , as well as $M_{23}C_6$, carbides can be present in Co-Cr-Mo casting cobalt alloys. The chemical composition analysis performed on micro-areas proved larger segregation of Mo into the interdendritic spaces (FIG. 4c, point 1-3 of the analyses).

The microstructure of the Co-Cr-Mo (EOS CobaltChromeMP1) alloy samples obtained by the direct metal laser sintering technique (DMLS) resembles "fish scales" in the light microscope images (FIG. 2a-d). The traces of the crossing laser beam are clearly visible. The fine-grained microstructure and multi-directionality of the occurring crystallization can be seen (FIG. 2d and FIG. 5b). One can notice that the grain boundaries exhibit geometrical diversity (FIG. 5). Also, the phenomenon of epitaxial dendrite growth is visible - the already present crystal growing through the consecutive melted layers.

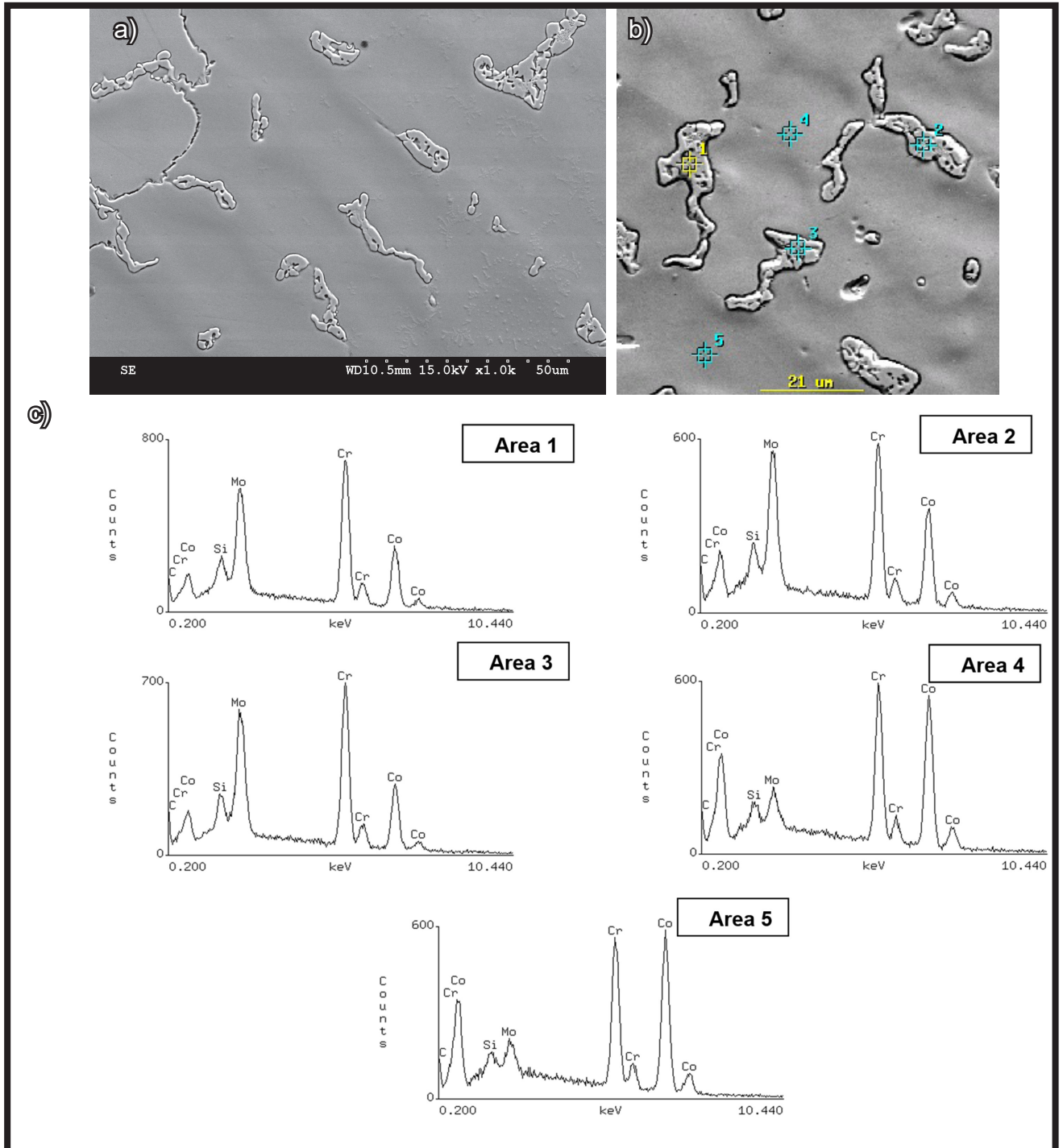


FIG. 4. Microstructure of Co-Cr-Mo alloy obtained by the lost-wax casting, SEM image (a) and X-ray spectra (c) of the places shown in the SEM microphotograph (b).

The dendrite axes formed in the microstructure stay in accordance with the heat removal direction during the crystallization process. The dendrites maintain their directions and run through the grain boundaries (FIG. 5a,b). The main dendrite axes are long and not much branched, which proves that the directional crystallization proceeds at a high rate [35,36]. The Co-Cr-Mo alloy samples obtained by DMLS have a very fine-grained microstructure which provides good mechanical properties of the alloy. Cobalt ensures high hardness, abrasive resistance and bending strength. The presence of chromium and molybdenum provides the alloy with good corrosion resistance.

The results of the EDS chemical composition analysis performed on the microsections of the Co-Cr-Mo (EOS CobaltChrome MP1) alloy obtained by the DMLS method are presented in FIG. 5 in the form of X-ray spectra. The EDS analysis of the sample's micro-areas did not reveal visible differences in the element content in the examined points, which confirms the homogeneity of the examined Co-Cr-Mo alloy, also established in the study [37]. No precipitation of carbide phases was observed for the samples obtained via the DLMS technique. During the DLMS process, the applied Co-Cr-Mo (EOS CobaltChrome MP1) powder was melted down.

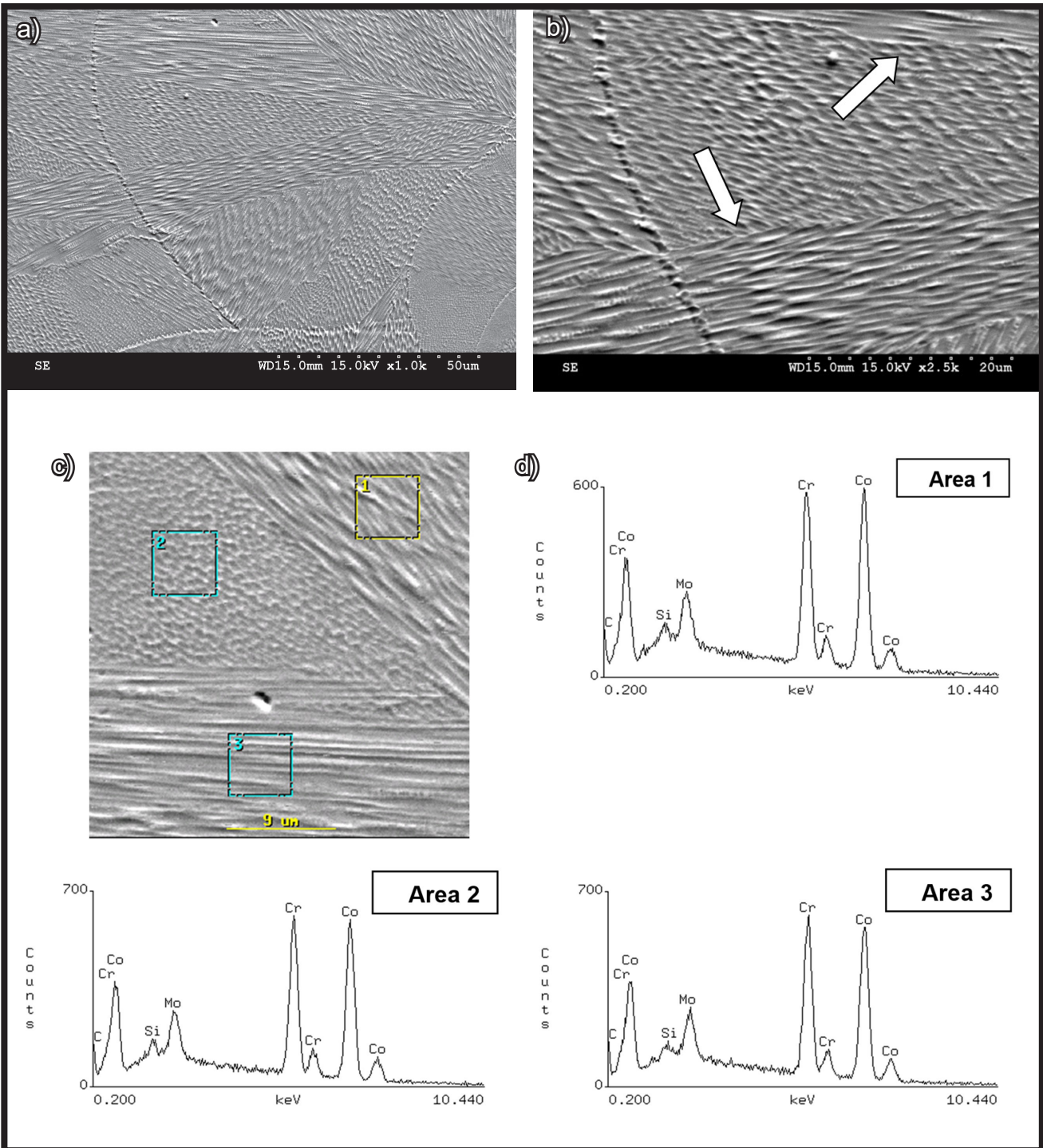


FIG. 5. Microstructure of Co-Cr-Mo alloy obtained by DMLS technique, SEM images (a, b) and X-ray spectra (d) of the places shown in the SEM photomicrograph (c).

TABLE 5. Hardness test results ($\overline{HV10}$) of Co-Cr-Mo alloys obtained by the lost-wax casting method and the DLMS technique.

Co-Cr-Mo samples obtained in the method	$\overline{HV10}$	$S_{(\overline{HV10})}$	δ_g	γ_g [%]
Lost-wax casting method	365	6.5	12.9	3.5
DLMS technique	474	5.4	10.6	2.2

Having in mind the microstructure observation results and the performed investigations [12, 14, 15] of the possible chemical inhomogeneities of the Co-Cr-Mo alloy obtained by the lost wax method and the finishing treatment (milling, grinding and polishing), the samples of both tested types underwent hardness measurements (HV10) in randomly selected areas. The mean hardness of the cast alloys was calculated, together with the standard deviation, the absolute limiting error (δ_g) and the relative limiting error (γ_g), according to the guidelines presented in the study [38]. A summary of the results is shown in TABLE 5.

The Co-Cr-Mo alloy samples obtained by the lost wax method exhibited the hardness of 366 HV10, whereas the mean hardness of the DMLS alloy equalled 477 HV10. The observed differences in the hardness values result from the fact that no significant differences in hardness in the whole volume are present in the EOS CobaltChrome MP1 alloy as it is chemically homogenous. In turn, the Co-Cr-Mo alloy samples obtained by the lost wax method display the diversified hardness: the lowest values were recorded in their central area, i.e. HV10 at the level of 340-350, while on their edges the values reached 360-370 HV10. This phenomenon is connected with the crystallization and the heat removal, the dendritic microstructure and the lack of chemical homogenization of the cast Co-Cr-Mo alloy.

Conclusions

Based on the performed microscopic observations (light microscopy and scanning electron microscopy, together with an EDS analysis in microsections) and the hardness measurements of the analysed alloys, the following conclusions were drawn:

The examined samples of the alloys Co-Cr-Mo (Wironit LA) and Co-Cr-Mo (EOS CobaltChrome MP1) were characterized by the dendritic microstructure.

The Co-Cr-Mo alloy samples had the matrix (dendrites) consisting of a chromium and molybdenum solution in cobalt, whereas, precipitations of carbide phases were present in the interdendritic areas, resulting from the chemical segregation of Mo and Cr.

The microstructure of the Co-Cr-Mo (EOS CobaltChrome MP1) alloy samples obtained in the DMLS technology exhibited fine grains and multi directionality of the alloy's crystallization. Also, the epitaxial growth of the dendrites was observed.

The samples obtained by the DLMS were characterized by the hardness higher than the cast alloy Co-C-Mo samples. The hardness values were directly affected by the fine-grained and more homogeneous microstructure of the examined DLMS material, as compared to the lost wax cast samples.

Acknowledgements

The authors would like to thank Patrycja Malmur for her help with laboratory preparation.

The work has been implemented within the framework of statutory research of AGH University of Science and Technology, contract No 16.16.110.663.

ORCID iDs

J. Augustyn-Nadzieja:  <https://orcid.org/0000-0002-3614-0609>

A. Szczotok:  <https://orcid.org/0000-0003-0680-0837>

References

- [1] Cervino G., Fiorillo L., Vladimirovna Arzukanyan A., Spagnuolo G., Ciccù M.: Dental Restorative Digital Workflow: Digital Smile Design from Aesthetic to Function. *Dentistry Journal* 7(30) (2019) 1-12.
- [2] Kashapov R.N., Korobkina A.I., Platonov E.V., Saleeva G.T.: The method of manufacture of nylon dental partially removable prosthesis using additive technologies. *IOP Conf. Series: Materials Science and Engineering* 69 (2014) 1-4.
- [3] Bilgin M.S., Baytaroglu E.N., Erdem A., Dilber E.: A review of computer-aided design/computer-aided manufacture techniques for removable denture fabrication. *European Journal of Dentistry* 10(2) (2016) 286-291.
- [4] Marciniak J., Kaczmarek M., Ziębowicz A.: *Biomaterials in Dentistry*, Publisher Silesian University of Technology, Gliwice 2008 (in Polish).
- [5] Hin T.S.: *Engineering Materials for Biomedical Applications. Biomaterials Engineering and Processing Series Vol. 1*. World Scientific Publishing Company, Singapore 2004.
- [6] Augustyn-Pieniążek J., Łukaszczyk A., Zapala R.: Microstructure and corrosion resistance characteristics of Co-Cr-Mo alloys designed for prosthetic materials. *Archives of Metallurgy and Materials* 58 (2013) 1281-1285.
- [7] Surowska B.: *Metallic biomaterials and the combination metal - ceramics in dental applications*, Publishing College, Lublin 2009 (in Polish).
- [8] Song B., Zhao X., Li S., Han Ch., Wei Q., Wen S., Liu J., Shi Y.: Differences in microstructure and properties between selective laser melting and traditional manufacturing for fabrication of metal parts: A review. *Frontiers of Mechanical Engineering* 10 (2015) 111-125.
- [9] Xiang D.D., Wang b P., Tan X.P., Chandra S., Wang C., Nai M.L.S., Tor S.B., Liu W.Q., Liu E.: Anisotropic microstructure and mechanical properties of additively manufactured Co-Cr-Mo alloy using selective electron beam melting for orthopedic implants. *Materials Science and Engineering: A* Vol. 765 (2019) 138270.
- [10] Barucca G., Santecchia E., Majni G., Girardin E., Bassoli E., Denti L., Gatto A., Iuliano L., Moskalewicz T., Megucci P.: Structural characterization of biomedical Co-Cr-Mo components produced by direct metal laser sintering. *Materials Science and Engineering: C* 48 (2015) 263-269.
- [11] Podrez-Radziszewska M., Haimann K., Dudziński W., Morawska-Sołtysik M.: Characteristic of intermetallic phases in cast dental CoCrMo alloy. *Archives of Foundry Engineering* 10(3) (2010) 51-56.
- [12] Zhou Y., Li N., Yan J., Zeng Q.: Comparative analysis of the microstructures and mechanical properties of Co-Cr dental alloys fabricated by different methods. *The Journal of Prosthetic Dentistry* 120(4) (2018) 617-623.
- [13] Loch J., Krzykała A., Łukaszczyk A., Augustyn-Pieniążek J.: Corrosion resistance and microstructure of recasting cobalt alloys used in dental prosthetics. *Archives of Foundry Engineering* 17(2) (2017) 63-68.
- [14] Augustyn-Pieniążek J., Kurtyka P., Sulima I., Stopka S.: Properties and tribological wear of materials used in dental prosthetics Co-Cr-Mo and Co-Cr-Mo-W alloys. *Archives of Metallurgy and Materials* 60(3A) (2015) 1569-1574.
- [15] Augustyn-Nadzieja J., Frocisz Ł., Krawczyk J., Pańcikiewicz K.: Analysis of properties and tribological wear of the Co-Cr alloys used for prosthetic constructions. *Tribology: theory and practice* 287(5) (2019) 5-12.
- [16] Örtorp A., Jönsson D., Mouhsen A., Vult von Steyern P.: The fit of cobalt-chromium three-unit fixed dental prostheses fabricated with four different techniques: A comparative in vitro study. *Dental Materials* 27(4) (2011) 356-363.
- [17] Zhou Y., Li N., Yan J., Zeng Q.: Comparative analysis of the microstructures and mechanical properties of Co-Cr dental alloys fabricated by different methods. *The Journal of Prosthetic Dentistry* 120(4) (2018) 617-623.
- [18] Szala M., Beer-Lech K., Gancarczyk K., Kilic O., Pędrak P., Ōzer A., Skic A.: Microstructural characterization of Co-Cr-Mo casting dental alloys. *Advances in Science and Technology Research Journal* 11(4) (2017) 76-82.
- [19] Padrós R., Punset M., Molmeneu M., Velasco A. B., Herrero-Climent M., Rupérez E., Gil F.J.: Mechanical Properties of CoCr Dental-Prosthesis Restorations Made by Three Manufacturing Processes. Influence of the Microstructure and Topography. *Metals* 10(6) (2020) 788-806.
- [20] Ciaputa T., Ciaputa A.: *Basics of prosthetic work, permanent work, frame dentures, combined work*, Publishing house Elamed, Katowice 2009 (in Polish).
- [21] Pietruski J.K., Pietruska M.D.: Materials and technologies used in modern prosthetics - advantages and disadvantages presented on the basis of a review of the literature and own experience. *Aesthetic dentistry* 9(3) (2013) 89-99 (in Polish).
- [22] Hajduga M., Aplikowska I.: Influence of pouring temperature on structural defects of metallic prosthetic restorations. *Arts and Crafts part II* (2011) 239-246 (in Polish).
- [23] Craig R., Powers J.M., Wataha J.W.: *Dental materials*. Medical Publishing House Urban & Partner, Wrocław 2000 (in Polish).
- [24] Siemiński P., Budzik G.: *Additive techniques Printing, 3D printers*. Publishing House of the Warsaw University of Technology, Warsaw 2015 (in Polish).
- [25] <https://cadxpert.pl/technologie-druku-3d/technologie-dmls/>
- [26] <https://drukarki3d.pl/oferta/dmls/>
- [27] Majewski S., Pryliński M.: *Materials and technologies of modern dental prosthetics*. Publishing house Czelej, Lublin 2013 (in Polish).
- [28] Rumińska M., Zarzecka J.: Contemporary prosthetic restorations of teeth, after root canal treatment - review of literature. *Implant prosthetics* 8/3 (2007) 33-36.
- [29] <https://dental.pl/produkt/wironit-la/>
- [30] https://drukarki3d.pl/wp-content/uploads/2020/09/eos_cobaltchrome_mp1_en.pdf
- [31] Świczko-Żurek B., Zieliński A., Ossowska A., Sobieszczuk S.: *Biomaterials*. Gdansk University of Technology, Gdańsk 2011 (in Polish).
- [32] Giacchi J.V., Morando C.N., Fornaro O., Palacio A.H.: Microstructural characterization of as-cast biocompatible Co-Cr-Mo alloys. *Materials Characterization* 62/1 (2011) 53-61.
- [33] Mendes S.N.P., Lins J.F.C., Mendes P.S.N., Prudente W.R., Siqueira R.P., Pereira R.E., Rocha S.M.S., Leoni A.R.: Microstructural Characterization of Co-Cr-Mo-W Alloy as Casting for Odontological Application. *International Journal of Engineering Research and Application* 7/3 (2017) 34-37.
- [34] Park J.B., Jung K-H., Kim K.M., Lee J-II., Ryu J.H.: Microstructure of As-cast Co-Cr-Mo Alloy Prepared by Investment Casting. *Journal of the Korean Physical Society* 72 (2018) 947-951.
- [35] Karpiński R., Walczak M., Śliwa J.: Tribological studies of cobalt alloys used as biomaterials. *Journal of Technology and Exploitation in Mechanical Engineering* 1/1 (2015) 17-32.
- [36] Mazurkiewicz A., Poprzeczka A.: Assessment of the quality of layers applied by laser metal deposition in LDT powder. *Coaches* 6 (2018) 591-596 (in Polish).
- [37] Wyszzyński D., Chuchro M.: *Manufacturing metal elements using the DMLS method*, Institute of Advanced Manufacturing Technologies, VIII Forum ProCAX, Sosnowiec 2009 (in Polish).
- [38] Maliński M.: *Selected problems of mathematical statistics in Excel and the Statistica Package*, Publishing house of the Silesian University of Technology, Gliwice 2015 (in Polish).